NAVAL POSTGRADUATE SCHOOL

MONTEREY, CALIFORNIA

THESIS

FIELD OBSERVATIONS AND SWAN MODEL PREDICTIONS OF WAVE EVOLUTION IN A MUDDY COASTAL ENVIRONMENT

by

Lincoln Thomas Trainor

June 2009

Thesis Advisor:	Thomas H.C. Herbers
Co Advisor:	Tim T. Janssen

Approved for public release; distribution unlimited

THIS PAGE INTENTIONALLY LEFT BLANK

REPORT DOCUMENTATION PAGE		*Form Approved OMB No. 0704-0188*

Public reporting burden for this collection of information is estimated to average 1 hour per response, including the time for reviewing instruction, searching existing data sources, gathering and maintaining the data needed, and completing and reviewing the collection of information. Send comments regarding this burden estimate or any other aspect of this collection of information, including suggestions for reducing this burden, to Washington headquarters Services, Directorate for Information Operations and Reports, 1215 Jefferson Davis Highway, Suite 1204, Arlington, VA 22202-4302, and to the Office of Management and Budget, Paperwork Reduction Project (0704-0188) Washington DC 20503.

1. AGENCY USE ONLY *(Leave blank)*	2. REPORT DATE June 2009	3. REPORT TYPE AND DATES COVERED Master's Thesis
4. TITLE AND SUBTITLE Field Observations and SWAN Model Predictions of Wave Evolution in a Muddy Coastal Environment		**5. FUNDING NUMBERS**
6. AUTHOR(S) Lincoln Thomas Trainor		
7. PERFORMING ORGANIZATION NAME(S) AND ADDRESS(ES) Naval Postgraduate School Monterey, CA 93943-5000		**8. PERFORMING ORGANIZATION REPORT NUMBER**
9. SPONSORING /MONITORING AGENCY NAME(S) AND ADDRESS(ES) N/A		**10. SPONSORING/MONITORING AGENCY REPORT NUMBER**

11. SUPPLEMENTARY NOTES The views expressed in this thesis are those of the author and do not reflect the official policy or position of the Department of Defense or the U.S. Government.

12a. DISTRIBUTION / AVAILABILITY STATEMENT Approved for public release; distribution is unlimited	12b. DISTRIBUTION CODE

13. ABSTRACT (maximum 200 words)

It is well known that the presence of mud deposits on the continental shelf can cause dramatic damping of ocean surface waves, but quantitive field observations are very scarce. Wave prediction models currently lack a physics-based representation of the mud-induced dissipation process, and hence the accuracy of wave predictions in muddy littoral environments is unknown. This thesis presents a comprehensive field data set for comparison with the operational wave model SWAN (Simulating Waves Nearshore). During February to March, 2008, an extensive array of 16 wave measuring instruments was deployed on the muddy shelf of Western Louisiana in depths ranging from 13 to 4 m. Box cores were collected at all instrument sites to characterize bottom sediment properties (Garcia-Garcia et al., 2008). Analysis of local wind sea events along two cross-shore transects shows a decay of waves from the deeper to the shallower instruments, with the strongest decay at the muddiest site. The wave spectra evolution shows strong decay of high-frequency wind sea spectral levels and weaker decay at the lower swell frequencies. The default bottom friction parameterization (the JONSWAP model with coefficient value $0.067\,m^2/s^3$) in the SWAN model generally yields reasonable estimates of nearshore wave heights that are sufficiently accurate for most operational Navy applications. However, the predicted cross-shore wave decay is more gradual than is observed and the model does not capture the spectra decay at high frequencies.

14. SUBJECT TERMS Ocean waves, Continental Shelf, Mud, Littoral, SWAN.			**15. NUMBER OF PAGES** 91
			16. PRICE CODE
17. SECURITY CLASSIFICATION OF REPORT Unclassified	**18. SECURITY CLASSIFICATION OF THIS PAGE** Unclassified	**19. SECURITY CLASSIFICATION OF ABSTRACT** Unclassified	**20. LIMITATION OF ABSTRACT** UU

THIS PAGE INTENTIONALLY LEFT BLANK

FIELD OBSERVATIONS AND SWAN MODEL PREDICTIONS OF WAVE EVOLUTION IN A MUDDY COASTAL ENVIRONMENT

Lincoln T. Trainor
Lieutenant Commander, Royal Australian Navy
B.Sc., University of New South Wales, 1998
Grad. Dip. Met., Bureau of Meteorology, 2002

Submitted in partial fulfillment of the
requirements for the degree of

MASTER OF SCIENCE IN PHYSICAL OCEANOGRAPHY

from the

NAVAL POSTGRADUATE SCHOOL
June 2009

Author: Lincoln Thomas Trainor

Approved by: Thomas H. C. Herbers
                 Thesis Advisor

                 Tim T. Janssen
                 Co-Advisor

                 Jeffrey Paduan
                 Chairman, Department of Oceanography

iii

THIS PAGE INTENTIONALLY LEFT BLANK

ABSTRACT

It is well kn own that th e presen ce of m ud deposits on the continental shelf can cause dram atic dam ping of ocean surface wave s, but quantitative field o bservations are very scarce. Wave prediction models currently lack a physics-based representation of the mud-induced dissipation process, and hence the accuracy of wave pre dictions in muddy littoral environments is unknown. This thesis presents a comp rehensive field data set for comparison with the o perational wave m odel SWAN (Si mulating Waves Nearshore). During February to March 2008, an extensive array of 16 wave m easuring instrum ents was deployed on the muddy shelf of Western Louisiana in depths ranging from 13 to 4 m. Box cores were collected at all instrum ent sites to characterize bottom sedi ment properties (Garcia-Garcia et al., 2008). Analysis of local wind sea events along two cross-shore transects shows a decay of wa ves from t he deeper to the sha llower instruments, with the strongest decay at th e muddiest site. The wave spectra evolution shows strong decay of high-frequency wind sea spectral levels and weaker decay at th e lower swell frequencies. The defa ult bot tom fric tion par ameterization (the JONSW AP model with coefficient value 0.067 m^2/s^3) in the SW AN model gene rally y ields reasonable estim ates of nearshore wave height s that are s ufficiently accurate for most operational Navy applications. Ho wever, the predicted cro ss-shore wave decay is more gradual than is ob served and the model doe s not captu re the spectra decay at high frequencies.

THIS PAGE INTENTIONALLY LEFT BLANK

TABLE OF CONTENTS

LIST OF FIGURES

x

THIS PAGE INTENTIONALLY LEFT BLANK

LIST OF TABLES

THIS PAGE INTENTIONALLY LEFT BLANK

ACKNOWLEDGMENTS

THIS PAGE INTENTIONALLY LEFT BLANK

I. INTRODUCTION

A. MOTIVATION AND OBJECTIVE

In September 1992, the U.S. Navy paper "F rom the Sea" signaled a shift in focus away from "operations on the sea to ward power projection and the em ployment of naval forces from the sea to influence events in the littoral regions of the world". This fundamental shift was a direct result of the changing strate gic landscape of the world and moving away from dealing with a global m aritime threat and toward projecting power and influence in regional areas. As a resu lt many countries now focus their efforts on a greater understanding of the littoral environment.

On October 17, 2007, t he Chief of Naval Op erations presented, "A Cooperative Strategy for the 21st Century Seapower," the first unified strategy for the maritime forces of the United States. This latest Maritime Strategic Concept reaffirmed its core capability of "Forward Presence" and listed one of its th ree strategic im peratives as the ability to "limit regional conflict with forward deployed, decisive m aritime power". The forecast of wave and surf cond itions ar e c ritical to th e succe ss o f m aritime f orces whic h ar e forward deployed in the littoral environment.

One exam ple of a m ilitary opera tion that is signif icantly af fected by wave conditions in the littoral environm ent is an am phibious landing. This was well highlighted in the delay of the D-Day inva sion of Nor mandy in 1944 due to high winds and seas. Wave and surf conditions can also be crucial in many other military operations such as special force's insertion, m ine warfare and hydrographic su rvey operations. Any military ope ration in th e litto ral en vironment c an be adv ersely af fected by the co astal wave climate.

In addition to wave prediction in littora l military operations, there a re many other applications inc luding r ecreational, commercia l and clim ate studies for which nearshore wave prediction is very i mportant. A common operational m odel used for wave prediction in the coastal region is known as Simulation Waves Nearshore (SWAN) (Booij et al., 1999). SW AN is a third generation numerical wave model developed to predict

short-crested waves in shallow water in th e presence of ambient currents. SW AN was designed to address the excessi ve computational demands of global wave models such as WAM (Kom en et al., 1994) and Wavewatch III (To lman and Chalikov, 1996) at high resolutions in coasta l re gions. SWAN incorporates m any complex processes including refraction, shoaling, wind forcing, non-linear in teractions and dissipa tion. Dissipation is further broken down into three m echanisms; bottom-induced dissipation, depth-induced breaking and whitecapping. The model treat s bottom -induced dissipation as the drag induced by a rigid sandy seaf loor (Booij et al., 1999) a nd employs the bottom friction model by Hasselmann et al. (1973). This us e of a bottom friction m odel does not allow SWAN to account for dissipation of wave s from a non-rigid m uddy sea floor. The absence of mud-related dissipation has been reported as a m ajor deficiency in S WAN (Dingemans, 1998). It has been shown in m any modeling studies (Gade, 1958; Dalrymple and Liu, 19 78; Ng, 2000) that su rface gravity waves can be dram atically damped by viscous mud. Recent field stud ies (Sheremet and Stone, 2003; Winterwerp et al., 2007; E lgar and Raubenheim er, 2008; Cuchia ra et al., 2009; Rogers and Holland, 2009) also show that waves can be dam ped by soft m ud layers. Muddy shorelines occupy an estim ated area of som e $170000km^2$ or 75% of the world's coastline between the 25^oN and 25^oS Latitudes (Flemm ing et al., 2000). W ith this widespread presence of muddy shorelines in the world it is im portant that nearshore wave models properly account for the mud-induced dissipation process.

This project will exam ine observations fr om a r ecent field experim ent, known as the Louisiana Mud Experim ent (MUDEX), on the m uddy continenta l shelf of Western Louisiana. An exten sive array o f inst ruments was deployed during the period of February to March 2008 to m easure in deta il the da mping of waves by a m uddy sea bed and investigates its im portance in the overall wave energ y balance. Observation al data from the experiment will be compared to SWAN model predictions.

B.   BACKGROUND

Extensive mud banks have been obser ved on continental shelves around the world. W ell known examples are the south-west Indian coast, north-e ast coast of S outh

America and the Gulf of Mexico. The soft bed has a prono unced effect on surface wave propagation in such areas a nd spectacular damping rates are ob served and rep orted, sometimes exhibiting nearly full attenuation of the surface wave field over just a few wavelengths (Gade, 1958; MacPherson, 1980). For instance, the damping characteristics of the Louisiana 'Mud-Hole' (92 ^{o}30'W) are us ed by lo cal fishermen as a shelter in case of an emergency in high seas.

This remarkable natural phenomenon led Gade (1958) to present a first theoretical analysis of wave dam ping characteristics of surface grav ity waves over mud, based on a two-layer representation of the m edium. He considered long-wave propagation on the surface of an invis cid upper fluid superposed o n a 'm ud' layer represented as a v iscous fluid. Later extensions include the propa gation of shorter waves over a sub-layer modeled as a viscous fluid (Dalrymple & Liu, 1978; Ng, 2000), visc o-elastic fluid or linear Voigt body sub-layers (MacPherson, 1980; Piedra-Cueva, 1993), or long waves over a Bingham -plastic (Mei & Liu, 1987). In effect, for these two-layer m odels, wave damping oc curs through the work done by the pressure gradient acting on the interf ace. Viscosity (r ather than e lasticity) p lays a c rucial ro le he re since it pu shes the f orcing relation away from exac t quadrature, in absence of which no attenuation would occur (MacPherson, 1980).

In recent years, observa tional studies (Sherem et an d Stone, 2003; E lgar and Raubenheimer, 2008; Cuchiara et al., 2009) s uggest the wave da mping problem may be more complex than a simple two layer fluid system. It has been generally thought that mud-induced dissipation only affe cts waves in the low frequency band of the wave spectrum because thes e waves are the on ly wa ves that interact efficiently with the bottom. Re sults from these recent studies suggest otherwise and show strong dissipation at both high and low frequencies. Sherem et and Stone (2003) propose that significant sediment resuspension and deposition proce sses m ay be t he cause of high frequency wave da mping and this is further su pported in J aramillo et al. (2009). The latter study shows that the m ud layer is m uch more dyna mic than first thought and is triggered by weather features such as frontal p assages causing near-bed sediment transport processes.

Such processes can include bed liquefaction, resuspension and advection. Such evidence suggests that mud resuspension and fluidization of the entire water column may also play a role in dissipation of waves in muddy coastal environments.

Although modeling studies have been ongoing since Gade (1958), comprehensive field observations remain scarce and the most notable observational studies have only taken place in the past decade. This has made it difficult to verify model results. Hsiao and Shemdin (1980) used two observations 3. 5km apart in Eastbay, Louisiana, from Tubman and Suhayda (1976) in 19.2 and 5.3m water depths. They showed that the proposed visco elastic model predicts wave energy decay much more effectively than a bottom friction model. It was noted that a high friction constant above 0.01 could not be justified in the study because of the very fine bottom sediment found in that area. This study was limited in observations and did not sufficiently capture the cross shore evolution of the wave field. Sheremet and Stone (2003) also conducted an experiment in the coastal waters of Louisiana. In this study, two observations were made at two sites, one located in a muddy environment, and the other in a sandy environment. They were located 150km apart in a water depth of 5m. The sites were considered to be subjected to similar wave generation and propagation conditions. Comparison of observations to the standard SWAN model showed severe over prediction of wave energy at the muddy site but found agreement at the sandy site. The results from Sheremet and Stone (2003) are somewhat inconclusive because of the large distance between the two observation sites (i.e., differences in wind conditions, wave climate).

A more detailed study of the cross-shore evolution of the wave field in shallow water (5m to 2m water depths) was recently conducted by Elgar and Raubenheimer (2008). Detailed observations across 1.8km of the Louisiana inner continental shelf were used to calibrate a new dissipation function in a non linear wave propagation model. While the model accurately reproduces the observed wave energy spectra transformation, these results were obtained in very shallow water, and may not apply to greater depths across the continental shelf where waves are dispersive and non-linear interactions are weak.

Another recent field data set exam ining cross-shore wave e volution in a m uddy environment was collected at Cassino Beach,   Brazil, in 2005. A collection of papers were publis hed recen tly that com pare this da taset to predictions of various two-layer boundary models (Cuchiara et al., 2009; Roge rs and Holland, 2009; Soltanpour et al., 2009). The array spanning 35km consisted of f our instruments: a directional waverider buoy in 25m water depth, an acoustic doppler prof iler in 8m, and two pressure gauges in 6m and 2m depths (Rogers and Holland, 200 9). A m ud layer of 40cm was observed between 9 to 15m water depths, placing all se nsors either offshore or inshore of the observed mud deposits. Using these field   observations, Rogers and Holland (2009) investigated dissipation by vi scous m ud with two for mulations in SWAN: (1) De W it (1995) with a m ud param eterization by W interwerp et al.   (2007) and (2) Ng (2000). Without m ud-induced dissipation SWAN over- predicted w ave ener gy at all sensors inshore of the m ud deposit zone. It only   showed com parable results during one high energy wave event. W hen the m ud for mulations were included, sim ulations m odestly under-predicted wave energy, sugge sting dissipation in these for mulations is too strong. Uncertainty in the rheology, distribution and depth of m ud are cite d as possible reasons for this difference. An inversion m ethodology was used to infer the mud distribution from the model that produces the observed wave heights. This methodology suggests the mud layer was up to 50% thinner than obser ved and m ore dynam ic than expected with the distribution extending further inshore.

C.   SCOPE

Field observations of mud-induced wave   dissipation are scarce and hence the performance of operational wave prediction   models in m uddy environm ents is poorly understood. This thesis presents a co   mprehensive field dataset to study the transformation of ocean surface waves across a muddy continental sh elf, in particular the expected strong wave dam ping. Observations from an extensive array of instruments deployed on the shelf of W   estern L ouisiana, during the ONR funded MUDEX Experiment, are com pared to predictions from the operational SW AN model to evaluate

the overall performance of SWAN in its standard configuration in a muddy environment. The bottom friction source term of Hasselmann et al. (1973) will be examined to see if there is an optimal tuning coefficient that can match field observations.

The two-dimensional array includes two cross-shore transects and one alongshore transect spanning a 40 x 25km area in depths ranging from 13m to 4m. Instruments were deployed at 16 sites, including two directional waverider buoys, six bottom tripods equipped with a pressure and velocity sensor and a current profiler, and eight bottom tripods equipped with a pressure sensor.

The thesis is organized in eight chapters. Chapter II describes the MUDEX Experiment including the location of the experiment, instruments used and data collection. Chapter III reviews methods used to analyze the field data. Chapter IV contains analysis of the observations. The implementation of the SWAN model is described in Chapter V. Results of model-data comparisons are examined in Chapter VI, focusing on four case studies, including local wind-sea and mixed swell-sea events with a range of wave directions and heights. This chapter also investigates model performance for different settings of the bottom friction parameter. Finally, Chapter VII contains a summary and conclusions.

II.   EXPERIMENT

A.   INTRODUCTION

The Louisiana Mud Experiment (MUDEX) was conducted in the northern Gulf of Mexico on the shelf of the western Louisiana coast, betw een Chenier Plain and Trinity Shoal, in the late winter/early spring of 2008 (Figure 1). Wave m easurements were collected at 16 sites in 4-13m dept h from Febr uary 09 to March 27. The instrum ents were deploy ed at specifically chos en site s to create two cross-s hore transects and one alongshore transect (Figure 2). Data were colle cted in two separate legs from February 09 to February 25 and March 04 to March 27, to allow f or the retrieval of records from instruments m idway through the experim ent. Initial deploym ent, redeploym ent and recovery of instrum ents were condu cted fr om the Universities National Oceanographic Laboratory System (UNOLS) Research Vesse l (R/V) PELICAN which was hom e ported in Cocodrie, Louisiana. Th e study was part of a larger field experiment, funded by the Office of Naval Res earch, to investigate the m echanisms of water wave dam ping over mud. Scientists from several un iversities an d ins titutions participated in the res earch effort including John Hopkins University, Ma ssachusetts Institute of Technology (MIT), Woods Hol e Oceanographic Institution (W HOI), Boston College, Louisiana State University (LSU), National Cheng Kung University, AOA Geophysics, the Scripps Institution of Oceanography (SIO) and the Naval Postgraduate School (NPS). This thesis is focused on the data collected by the NPS group in collaboration with the SIO and AOA groups.

B.   FIELD SITE

The west Louisian a coast is a v ery active segment of coastline at the co nfluence of the Mississippi River outflow and the Gulf of Mexico. Th e area is under the influence of the Atchafalaya Riv er (Figu re 1), the larg est distributary of th e Mississippi River, which captures about 30% of its discharge, w ith an average sedim ent load of 84 m illion metric tons per year (S heremet and Stone, 2003). Mud plum es, which are normally confined shoreward of the 10m isobaths, vary in size and extent base d on the severity of

the weather conditions. Peak mud plume activity occurs in late winter and early spring months, coinciding with high river discharge   levels and intense cold fronts (Mossa and Roberts, 1990). Figure 3 illustrates a mud plume observed during the experiment. The image was taken during the recovery cruise on the second leg of the experiment and illustrates how much the water column can change from mud fluidization. A significant cold front had passed through the area a week prior to the recovery cruise and may have contributed to the mud suspension. A nearby waverider buoy, in a water depth of 13m, recorded waves reaching nearly three meters during the peak of the storm.

The MUDEX study area, shown in Figure 2, displays a coastline that is predominantly NW/SE. The bathymetry contours parallel the coastline along the Chenier Plain until the Trinity Shoal. At the Trinity Shoal, the contours curve south to approximately 40km offshore and then turn east. The Trinity Shoal has a minimum depth of approximately 5m.

C.   INSTRUMENTS AND DATA COLLECTION

The array consisted of two cross-shore transects and one alongshore transect. The cross-shore transects named, "Western" and "Central" respectively, relative to their position in the array, were approximately 18km long and span water depths ranging from 4m to 13m. The alongshore transect, named "Eastern", was approximately 25km long and extends from Trinity Shoal (5m depth) westward to about 12m depth. In total, eight bottom tripods with a pressure sensor (designated as PA-x where x is the site number), six bottom mounted frames each containing a pressure-velocity sensor and a current profiler (designated PV-x), and two surface-following waverider buoys (designated DW-x) were deployed (Table 1 and Figure 2).   The array was designed to provide a comprehensive field dataset on the evolution of surface waves across a muddy shelf. The instruments were recovered and redeployed in the same positions during a turna round cruise in late February 2008 to retrieve data records from the first leg.

1.   Bottom Pressure Sites

The eight bottom pressure sensors were each mounted on a fiberglass tripod fitted to a recovery line with a surface float (Figure 4). A small acoustic pinger was also fitted

to the tripod to loca te it underwater during recovery. They were deployed from the R/V PELICAN using differentia l GPS for precise   positioning with accura cy to within 5m . The instrument is a self contained, battery powered and internally recording package with a Setra 270 capacitance-type pressu re gauge (d eveloped and built at SIO). The pres sure (PA) tripods were deployed at various si   tes to m easure wave-induced near-bottom pressure fluctuations in water depths of 4 to 10m. Three pressure sensors were located on the western transect (sites 3, 5 and 6), thr ee on the central transect (sites 8, 10 and 11), and two on the eastern transect (sites 14 and 15). Two pressure sensors, at sites 6 and 11, were not recovered during the turnaround crui   se as they were possibly dragged by the high volume of fishing vessels in the area.   Also a third sensor, at site 10, w   as not recovered during the final recovery cruise   for the sam e reason. The pressure records were recorded internally at a continuous sampling rate of 2 Hz.

2.   Bottom Pressure and Velocity Sites

The six Nortek Vecto r pressure-veloc ity instrum ents were each m ounted on a fiberglass tripod in a sim ilar way t o the pressu re sensors. The instrum ent contains an Acoustic do ppler velo cimeter that m easures three- component veloc ity f luctuations at a single point above the instrum ent and a pressu re gauge. T he fiberglass tripod was also equipped with a Nortek Aqua dopp current profiler, to prov ide redundant pressure and velocity measurements in case the V ector instrument fails. The tripod was m ounted on a 1.1m tall metallic frame to keep the instruments from sinking into the mud (Figure 5). To aid recovery, all tripods were fitted with an acoustic re lease mechanism, a small acoustic pinger, and a recovery line with su rface floa t. The near-bo ttom pressure and horizo ntal velocity measurements collected at six sites, in depths of 6 to 12m, were used to estim ate wave-height and directional spectra through te chniques described in Chapter III. Two pressure-velocity tripods were located on the western transect (sites 2 and 4), two on the central trans ect (s ites 7 and 9), and two on the eastern tran sect (sites 13 and 16). The Vector pressure and velocity da ta were recorded internally in bursts of 68 minutes, every 4 hours, at a sampling rate of 2 Hz. The Aqua dopp wave data were recorded internally in bursts of 34 minutes, every 1 hour, at a sampling rate of 1 Hz.

3. Waverider Buoys

Two 0.9m diam eter su rface-following Da tawell Direction al W averider buoys were deployed in water depths of 11m and 13.5m (Figure 6). Each buoy is equipped with a three-com ponent accelerom eter, a com pass, and a tilt sensor to m easure vertical and horizontal s ea surface displacem ents in an ab solute (nor th, west, vertical) coordinate frame. W averider buoys are capable of produc ing wave-height and di rection spectra in real-time us ing their onboard m icroprocessor, however, this feature was not used and instead this inf ormation was caref ully com puted from the post-processed displacement data. The vertical displacement data were us ed to estimate wave-height spectra and both the horizon tal and vertical disp lacements were used to estim ate dir ectional spe ctra through techniques discussed in Chapter III. One buoy was located at th e most offshore site of the western transect (site 1) and the other buoy at th e deep end of both the central and eastern transects (site 12) (Figu re 2). Th e displacement data was recorded in ternally in 30 minute segments continuously at a sampling rate of 1.28 Hz.

4. Other Measurements

Box core observations of bottom sedim ents were taken at each site d uring the deployment and recovery cruises by Geologist , Dr Anna Gar cia-Garcia, t o char acterize the rheology of m ud in the ar ea (Figure 7, 8 and 9). These sam ples were also analy zed using a Rheometer in the Department of Civil Engineering at John Hopkins University by Khatoon Sabouri-Shargh to estimate viscosity in the mud layer.

Wind observations were taken by an anem ometer on a m eteorological buoy (Figure 10) that was deploye d by Dr. John Trowbridge from W HOI during MU DEX. The m eteorological buoy was located between sites 5 and 6 on the western transect (Figure 2). Mean wind speed and direction observations were recorded at 3m above sea level at five m inute intervals from Februa ry 14 to the end of MUDEX. These wind measurements (provided by Dr. Janet Freder icks from W HOI) were co rrected to 1 0m elevation (U_{10}) using a standard logarithm ic wi nd profile and Charnocks's (1955) estimate of the sea surface roughness (using a coefficient value of 0.0144).

10

A bathym etry grid with a resolution of 0.001 degrees w   as assem bled for the
Louisiana coastal region by Paul Jessen (F   igure 2) at NPS from   the NOAA National
Ocean Survey (NOS) Hydrographic database.   Bathymetric data was extracted usin g the
NDGC GEODAS tool.

Site Number	Instrument Type	Latitude (Deg North)	Longitude (Deg West)	Depth (m)
1 D	W	29.444	92.632	13.0
2 PV		29.477	92.625	12.39
3 PA		29.504	92.603	10.80
4 PV		29.523	92.599	9.39
5 PA		29.539	92.595	Not recovered
6 PA		29.553	92.592	6.00
7 PV		29.424	92.5	11.37
8 PA		29.453	92.494	10.85
9 PV		29.491	92.475	8.40
10 PA		29.518	92.463	5.28
11 PA		29.529	92.459	Not recovered
12 D	W	29.33	92.489	11.5
13 PV		29.327	92.432	9.83
14 PA		29.308	92.39	8.75
15 PA		29.308	92.317	7.38
16 PV		29.294	92.265	6.91

Table 1.   Instruments deployed during MUDEX. Depth for the PA and PV instruments are
an estimated average from the pressure time series collected during the first leg.
Depth for the DW buoys is estimated from the high resolution bathymetry.

Figure 1.   Location of the MUDEX Experiment in the northern Gulf of Mexico.
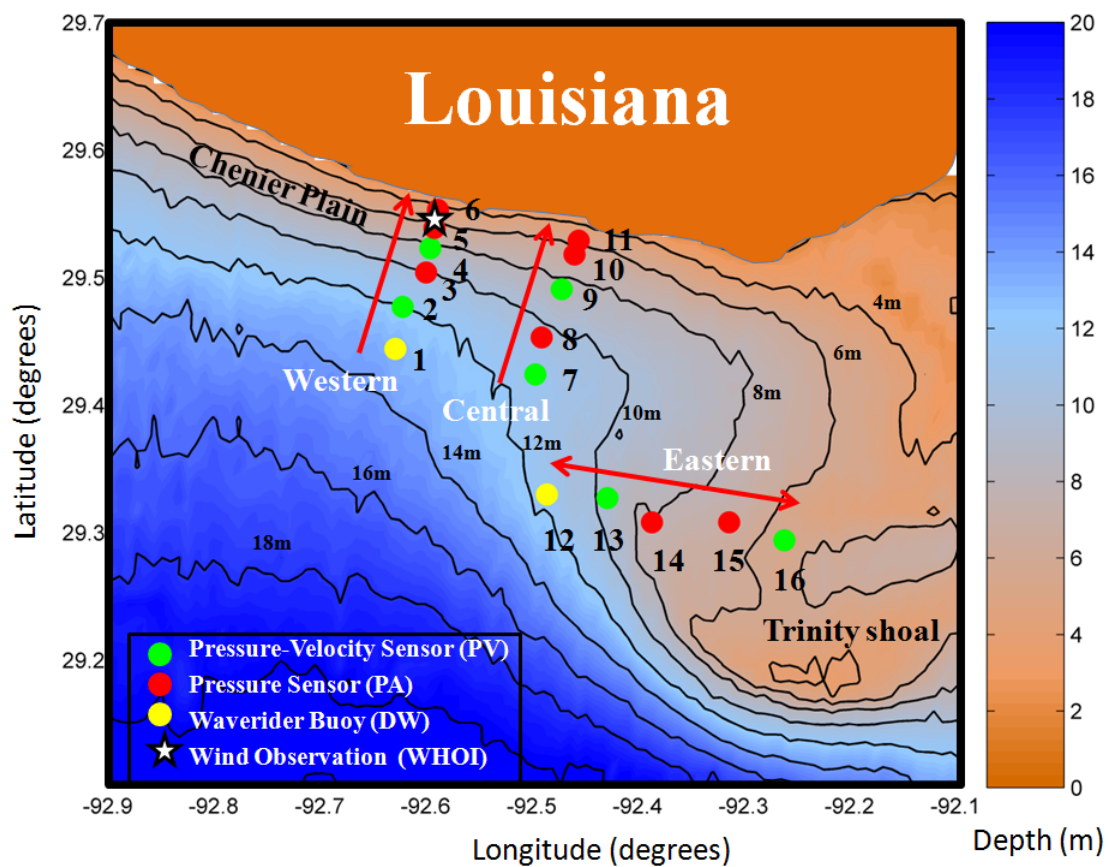
Figure 2.   Bathymetry of the MUDEX area and location of instruments used in the experiment.

Figure 3.   Image of mud plume taken during the recovery cruise of MUDEX.

Figure 4.   Recovery of a pressure sensor (PA) tripod during the final recovery cruise of MUDEX. The pressure sensor is fitted to a fiberglass tripod equipped with lead feet to ensure stability on the ocean floor. The small cylinder to the right of the pressure sensor is an acoustic pinger that helps locate the instrument.

Figure 5.   Recovery of a pressure-velocity frame on the final cruise of MUDEX. The Nortek Vector pressure-velocity (PUV) instrument with a three-pronged acoustic receiver probe extends vertically upward from the tripod. The pressure sensor is located at the base of this probe. The Aquadopp current profiler is the horizontal cylinder mounted on the left side of the tripod. The acoustic release mechanism is located below the center of the tripod and attaches the tripod to a metallic frame equipped with weights to ensure stability on the ocean floor. The small cylinder above the right leg of the tripod is an acoustic pinger that helps locate the instrument.

Figure 6.   Datawell Waverider buoy (DW) after recovery on the final cruise of MUDEX. Both buoy's were fitted with an anti-spin triangular frame to reduce risk of damage from collisions.

Figure 7.   Box core taking a mud sample of the sea floor during the recovery cruise of MUDEX (Top panel). A close up of a sample, shown in the Bottom panel, indicates a few centimeters of very soft fluid mud overlying soft mud.
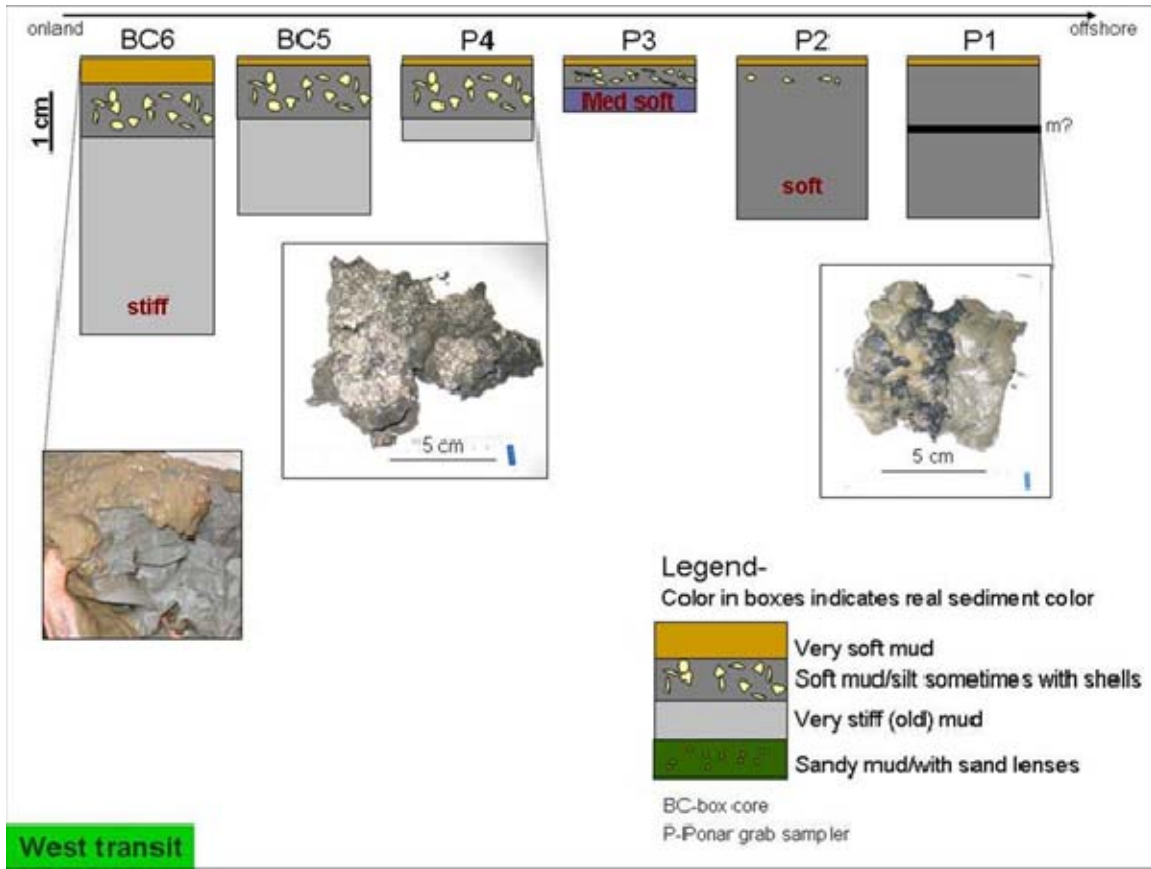
Figure 8.   Box cores characterizing sediment properties at all instrument sites along the Western Transect. A very thin film of soft fluid mud is observed at all sites. Sites are designated BC-x or P-x, where BC represents Box Core, P represents Ponar grab sampler and x is the site number. (From Garcia-Garcia et al., 2008)
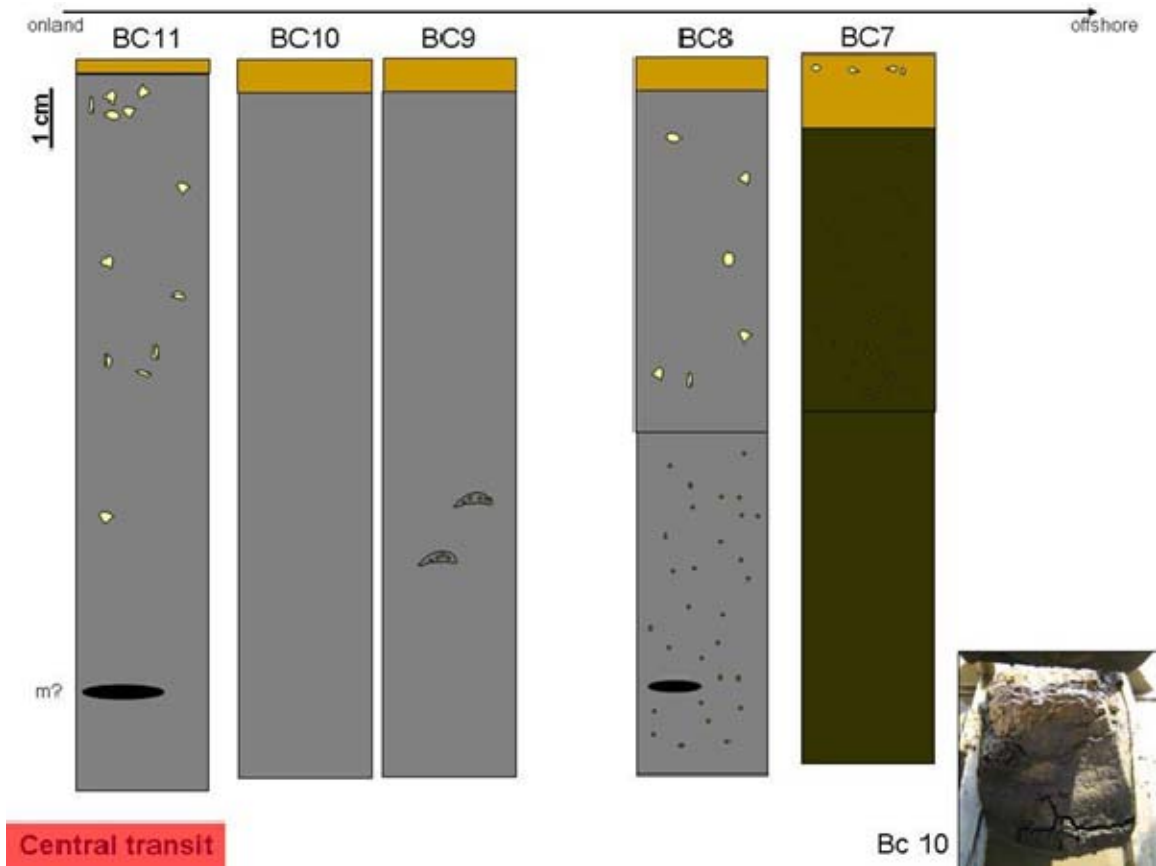
Figure 9.   Box cores characterizing sediment properties at all instrument sites along the Central Transect. The fluid mud is thicker than observed along the Western Transect, possibly because of the proximity of the Atchafalaya river. Site notation is same format as Figure 8. (From Garcia-Garcia et al., 2008)

Figure 10.   Meteorological buoy deployed by WHOI during MUDEX. The anemometer is 3m above sea level and is the tallest sensor attached to the buoy. (From Dr. Janet Fredericks at WHOI)

THIS PAGE INTENTIONALLY LEFT BLANK

III. WAVE DATA ANALYSIS

A. INTRODUCTION

This chapter outlines the methods used to obtain surface elevation frequency and directional wave spectra from the various instruments deployed during MUDEX. It also details techniques used to calculate common parameters such as significant wave height, wave peak period and mean wave direction.

B. DESCRIPTION OF THE WAVE FIELD

1. Surface Elevation Spectrum

To estimate the surface elevation spectrum $E(f)$ from the near-bottom pressure measurements at the PA and PV sites, linear wave theory was used to account for vertical attenuation of the wave motion. The linear transfer function between sub-surface pressure (in units of equivalent water column height) and surface elevation is given by:

$$H(f) = \frac{\cosh kh}{\cosh kd} \tag{1}$$

where h is the total water depth, and d is the height of the pressure sensor above the sea floor. The wavenumber k is given by the dispersion relation $(2\pi f)^2 = gk \tanh kh$. An estimate of the sea surface spectrum is obtained by multiplying the subsurface pressure spectrum $E_p(f)$ by the squared transfer function:

$$E(f) = |H(f)|^2 E_p(f) \tag{2}$$

A simpler procedure applies to the Waverider Buoy DW sites. The spectrum of the vertical buoy displacement data yields a direct estimate of $E(f)$.

2. Frequency-directional Spectrum

The directionality of waves is often described by the mean direction $\theta_{mean}(f)$ as a function of frequency, that can be estimated with a high degree of accuracy from

directional wave buoys (e.g., O'Reilly et al., 1996) and pressure-velo   city sensors (e.g.
Herbers et al., 1999). It is commonly define   d in term s of the fi rst order directional
moments a_1 and b_1 of the frequency-directional w   ave spectrum $E(f,\theta)$ (Longuet-
Higgins et al., 1963):

$$\theta_{mean}(f) = \tan^{-1}\left(\frac{b_1(f)}{a_1(f)}\right) \tag{3}$$

with

$$a_1(f) \equiv \int \frac{\cos\theta E(f,\theta)d\theta}{E(f)} \tag{4}$$

$$b_1(f) \equiv \int \frac{\sin\theta E(f,\theta)d\theta}{E(f)} \tag{5}$$

In this definition, $\theta_{mean}(f)$ represents the direction of the wave energy flux as a
function of frequency, and thus has a sim   ple physical interpretation. The m   oments a_1
and b_1 are readily determ ined from either   surface x,y,z displacem ents or sub-surface
p,u,v measurements. For the waverider (DW) buoys a_1 and b_1 are related to the sp ectra
and cross spectra of the horizontal and vertic al displacements by L onguet-Higgins et al.,
(1963):

$$a_1(f) = \frac{iQ_{xz}(f)}{\left\{C_{zz}(f)\left[C_{xx}(f)+C_{yy}(f)\right]\right\}^{\frac{1}{2}}} \tag{6}$$

$$b_1(f) = \frac{iQ_{yz}(f)}{\left\{C_{zz}(f)\left[C_{xx}(f)+C_{yy}(f)\right]\right\}^{\frac{1}{2}}} \tag{7}$$

24

Where C_{ij} and Q_{ij} indicate the co- and quadrature spectrum between measurements i and j. Similar relations exist for pressure and velocity (PV) measurements in terms of the normalized co-spectra of the horizontal velocity components u and v and pressure p (e.g., Herbers et al., 1999):

$$a_1(f) \equiv \frac{C_{pu}(f)}{\left\{C_{pp}(f)\left[C_{uu}(f)+C_{vv}(f)\right]\right\}^{\frac{1}{2}}} \qquad (8)$$

$$b_1(f) \equiv \frac{C_{pv}(f)}{\left\{C_{pp}(f)\left[C_{uu}(f)+C_{vv}(f)\right]\right\}^{\frac{1}{2}}} \qquad (9)$$

Finally, to initialize the SWAN model with an offshore boundary condition, a full frequency-directional wave spectrum $E(f,\theta)$ is required. This spectrum was estimated from the buoy measurements at site DW12 using the Maximum Entropy Method (MEM) of Lygre and Krogstad (1963). This method uses the full cross spectral matrix of the buoy measurements.

3. Bulk Parameters

In addition to the surface elevation frequency and directional spectra, the peak wave period T_p, peak wave direction D_p and significant wave height H_s were calculated. The peak wave period, T_p, and wave direction D_p, were taken as the period and mean direction corresponding to the frequency band with the maximum spectral density. The significant wave height was calculated using the standard definition:

$$H_s = 4\sqrt{\int_{0.05\,Hz}^{0.25\,Hz} E(f)\,df} \qquad (10)$$

where the spectral density, $E(f)$, is integrated across a wide frequency band from 0.05 Hz to 0.25 Hz. Higher frequency components are not included to avoid errors associated with the strong attenuation of the pressure signals at the deeper PV and PA sites.

The significant wave height was also cal culated for the sea and swell components separately to investigate differences in the transformation of longer wavelength swell that feel the bo ttom across the shelf and shorter wavelength sea that are less affected by th e seafloor. These computations use the same definition as (8) but with restricted frequency bands of 0.05 Hz to 0.15 Hz for the swell com ponent and 0.15 Hz to 0.25 Hz for the sea component:

$$H_s(swell) = 4\sqrt{\int_{0.05\,Hz}^{0.15\,Hz} E(f)\,df} \tag{11}$$

$$H_s(sea) = 4\sqrt{\int_{0.15\,Hz}^{0.25\,Hz} E(f)\,df} \tag{12}$$

C.   SPECTRAL ANALYSIS

To facilitate comparisons of different instruments, the data f rom each instrum ent was processed for a common 68 m inute tim e in terval that is long com pared with the propagation time of swell to cross the instru mented transects, wh ile wind-sea conditions usually are reasonably stationary over an hour. The PV se nsors collected data in 68.2 minute bursts every 4 hours while the DW buoys and P A sensors collected data continuously. To yield a comm on tim e inte rval, the DW buoy dat a (with a different sample rate, see below) was processed in 70 minute bursts every 4 hours and the PA sensor was processed in 68.2 minute bursts every 4 hours to match the PV sensor.

Spectra (and cross-spectra) were com puted for the PA and P V sensors from 68.2 minute records (8192 points with a sam ple interval of 0.5 seconds) using a segm ent length of 128 points and a 50% overlap, res ulting in 12 8 degrees o f freedom for a frequency resolution of 0.015625 Hz. The DW buoy data analysis wa s performed on 70

minute records (5376 points) with a sam ple interval of 0.78 seconds, using a segm ent length of 128 points and a 50% overlap, yieldi ng 84 degrees of freedom and a frequency resolution of 0.01 Hz.

The mean wave direction $\theta_{mean}(f)$ as com puted from ensemble averages of the directional moments (a_1, b_1) in (3) are weighted by the energy density $E(f)$ using the relations from equations 4 and 5 for the DW sensors and equations 6 and 7 for the PV sensors. Fo r each instrum ent site this pr ocess yielded average wa ve spectra and m ean wave directions (as a function of frequency) at 4 hour intervals starting at 00:00, 04:00, 08:00, 12:00, 16:00, 20:00 GMT over the entire experiment period.

THIS PAGE INTENTIONALLY LEFT BLANK

IV. OBSERVATIONS

A. INTRODUCTION

In this chapter, wind and wave observat ions are presented for the first leg of MUDEX. The second leg is not included   in the observ ational an alysis be cause th e inshore sensor at site 10 was   not recovered during the final r ecovery cruise. Site 10 is considered rather special, as it rep   resents the most inshore operational sensor on the muddier central transect where the strongest wave damping is observed.

B. WIND OBSERVATIONS

A time series for wind observations during the first leg of MUDEX is presented in Figure 11. Surface analysis weath   er charts fo r the northern Gulf of Mexico are also presented in Figures 12, 13, and 14 to provide   a greater insight into the wind field. As specified in Chapter II, wind observations   were taken by a single m eteorological buoy, from WHOI, located between sites 5 a   nd 6 on the w   estern transect. A second meteorological station operated by Louisiana   State University (LSU) was loca ted 5 0km east of the WHOI buoy. Howeve   r, since th e MUDEX area is relatively sm   all, and similarity between wind observations at the   two stations (not s   hown) suggest fairly homogeneous wind conditions, only data from the WHOI buoy was used in this study.

It is evident in the W   HOI buoy wi nd obser vations (Figure 11) that there were three distinct frontal passages during the fi rst leg, each accompanied by a sudden ch ange in wind direction observed on February 18, 22, and 26 (Figure 11 Bottom Panel). There is also another less pronounced frontal system that passed the area during February 17. It is represented by a brief wind change and si gnificant increase in wind speed (Figure 11). Other fronts crossed the area   early on February 13 and Ma   rch 4 (not shown) and the effects of these can be seen in the wave observations (Figure 15, 16, and 17). It appears that fronts generally cross the area every four to five days. Examining wind speed for the frontal events shown in Figure 11, it is evident that the first, second and fourth fronts are

much stron ger than th e third f ront with winds speeds greater than 12 m /s (>23kts). Interestingly, the first front has the stronge st winds before the frontal passage, whereas the second and fourth front have stronger winds after the frontal passage.

Figure 12 shows surface weather ch arts for the first front at 0 600Z and 0900Z on February 17 (Figure 12). The chart at 0600Z shows initial strong to gale force wind conditions offshore of the MUDEX area, before the front, from wind barbs displaying 25-35kts. Then as the front crosses the area at 0900Z the winds modera te briefly across the area. The wind freshens again on February 18 as a second front (surface weather chart not shown) quickly moves into the area tightening the pressure gradient and reflecting the increase in wind speed shown in the time series (Figure 11 Top Panel).

The third frontal passage is displayed in weather charts at 1200Z and 1500Z on February 2 2 (Figur e 1 3). The c hart at 120 0Z shows initial weak wind cond itions throughout the area before the front. The winds then rem ain relatively light as the front crosses the area, shown in the chart at 1500Z. However, this is only short lived as a ridge of high pressure moves into the area behind the front causing winds to freshen by late on February 22.

The fourth front is shown in weathe r charts at 0900Z and 1200Z on February 25/26 (Figure 14). The chart at 0900Z shows strong wind c onditions of 20-25kts offshore before the front. However, these conditions are not as strong as the wind conditions before the first front. This can be explained by the fact that the low pressure system passing north o f the area is m uch we aker in the fourth frontal case. W inds become strong to gale force during the frontal passage show n in chart 1200Z with a 40kt wind barb offshore of t he MUDEX area. W inds rem ain quite strong and offshore until the m iddle of February 27 (Figure 11 Top Pane l) as the intense high pressure system behind the front combines with the low pressure system north of the area (not shown).

C. WAVE OBSERVATIONS

1. Cross-shore Transects

Time series of wave observations for the western and central tran sects are displayed in Figures 15 and 16. W ave observations include significant wave height H_s, peak wave period T_p and peak wave direction D_p.

Wave height observations al ong the western transect (F igure 15 Top Panel) show a general d ecay as waves propag ate from the deepes t sensor DW 1 t o the sh allowest sensor PA6. However, a m uch stronger d ecay is observed along the central transect (Figure 16 Top Panel) between sites DW 12 and PA10 with reductions in wave height by as m uch as 45%. This m ay be a result of the closer proxim ity to the outflow of the Atchafalaya river producing a thicker layer of soft mud on the central transect (Figure 9). The frontal passages are reflect ed in the wave heights of both transects w ith strong to gale force wind conditions before the first front creating the largest wave heights during February 17. The passage of the third weaker front and associated low pressure system is responsible for the slight rise in wave he ights during February 21 and 22. The fourth front caused the rise in wave heights during February 26.

Peak wave period observati ons, in Figures 15 and 16 (Middle Panel), are very similar for the two transects and show a range in period betw een 4 and 10 seconds. The peak period generally rem ains below 8 sec onds as severe storm s that produce longer swells in the Gulf of Mexico are uncommon during the winter months.

The peak wave directions in Figures 15 and 16 (Bottom Panel) show a general southerly direction except after strong fr onts when the wind turns offshore causing northerly (i.e. fetch-limited) wave directions for up to 24 hours.

2. Alongshore Transect

Time series for wave observations on the eastern transect are shown in Figure 17 (Top Panel). As this transect runs alongshore into Trinity S hoal, it does not display the

same decay in wave heights as the cross sh   ore trans ects. Wave   heights are relatively similar at all sites and reflect the frontal   activity. Peak period and direction are very similar to the cross shore transects.

### 3.	Sea and Swell Contributions

As discusse d in Chapter III, the bu   lk param eter of significant wave height was also separated into sea and swell com   ponents. These components were calculated to better understand the cross-shore decay in diff   erent parts of the wave   spectrum when waves m oved inshore along the cross-shore tran   sects. Tim eseries of the sea and swell components of wave height for the central tr ansect are presented in Figure 18. W hereas the longer wavelength swell com   ponent m ay be expected to be affected m   ore by the seafloor boundary laye r processes, surprisingly the sea   component of the wave height experiences significantly greater decay than the swell com ponent. It is also evident that the frontal activ ity has more of an effect   on the sea com ponent with the wave heights more closely aligned to the wind observations.
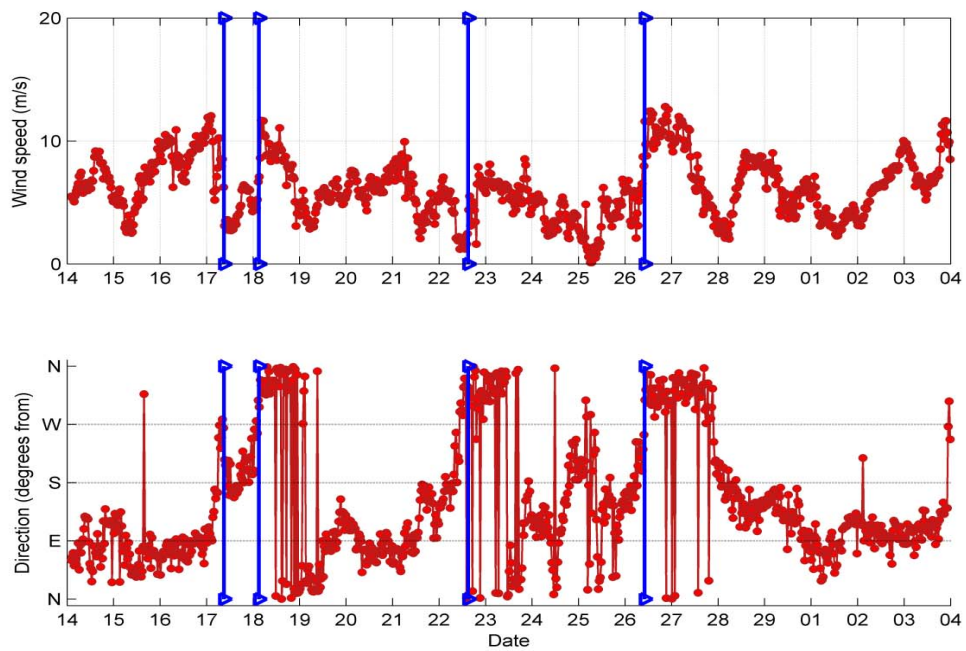
Figure 11.   WHOI wind observations for the first leg of MUDEX. Cold fronts are marked by blue vertical lines. (Courtesy of Dr. John Trowbridge and Dr. Janet Fredericks at WHOI)
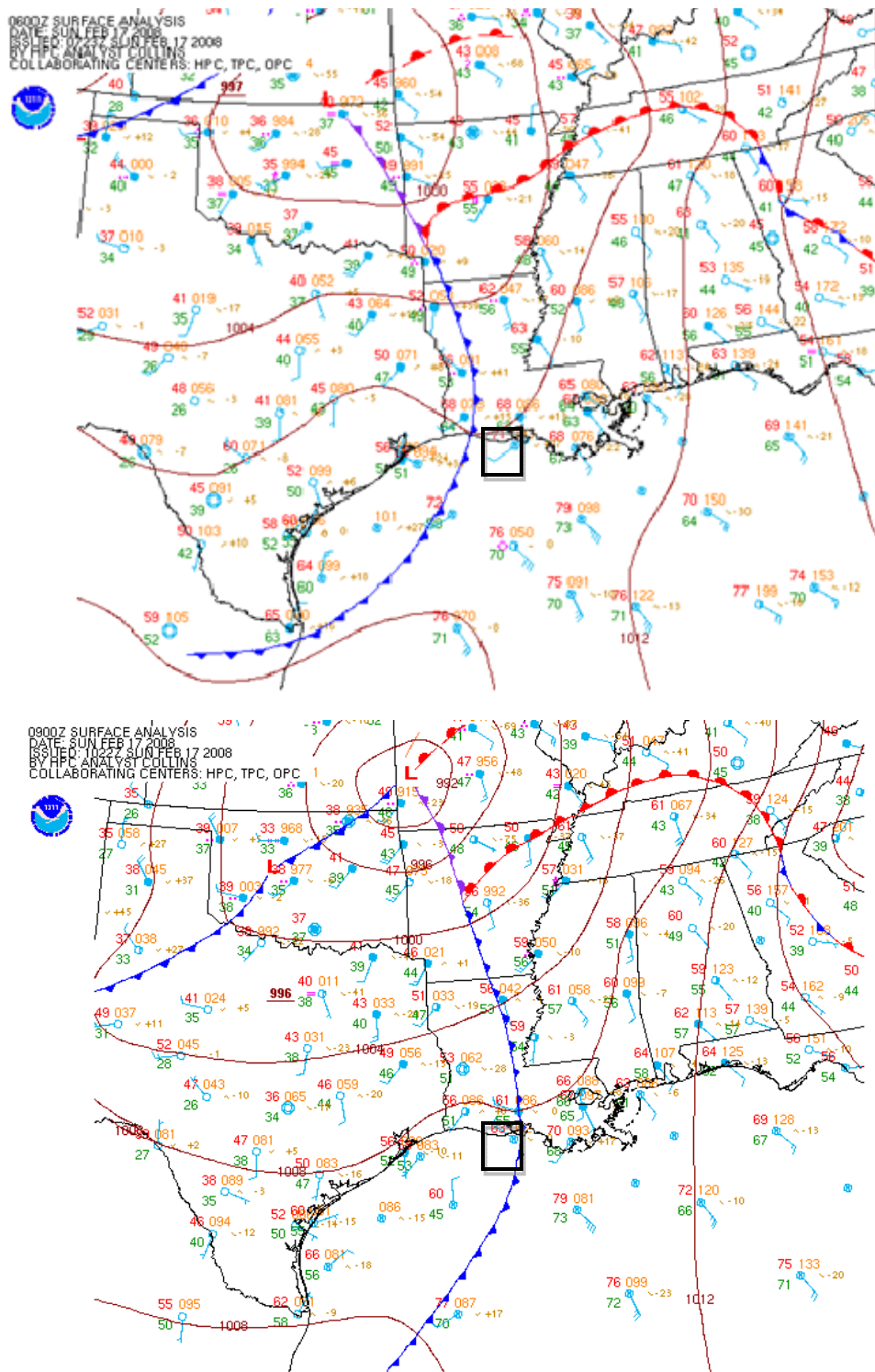
Figure 12.   Surface Analysis Weather Charts for February 17, 2008: 0600Z (Top panel) and 0900Z (Bottom panel). The experiment site is indicated with a black square. (From nomads.ncdc.noaa.gov)
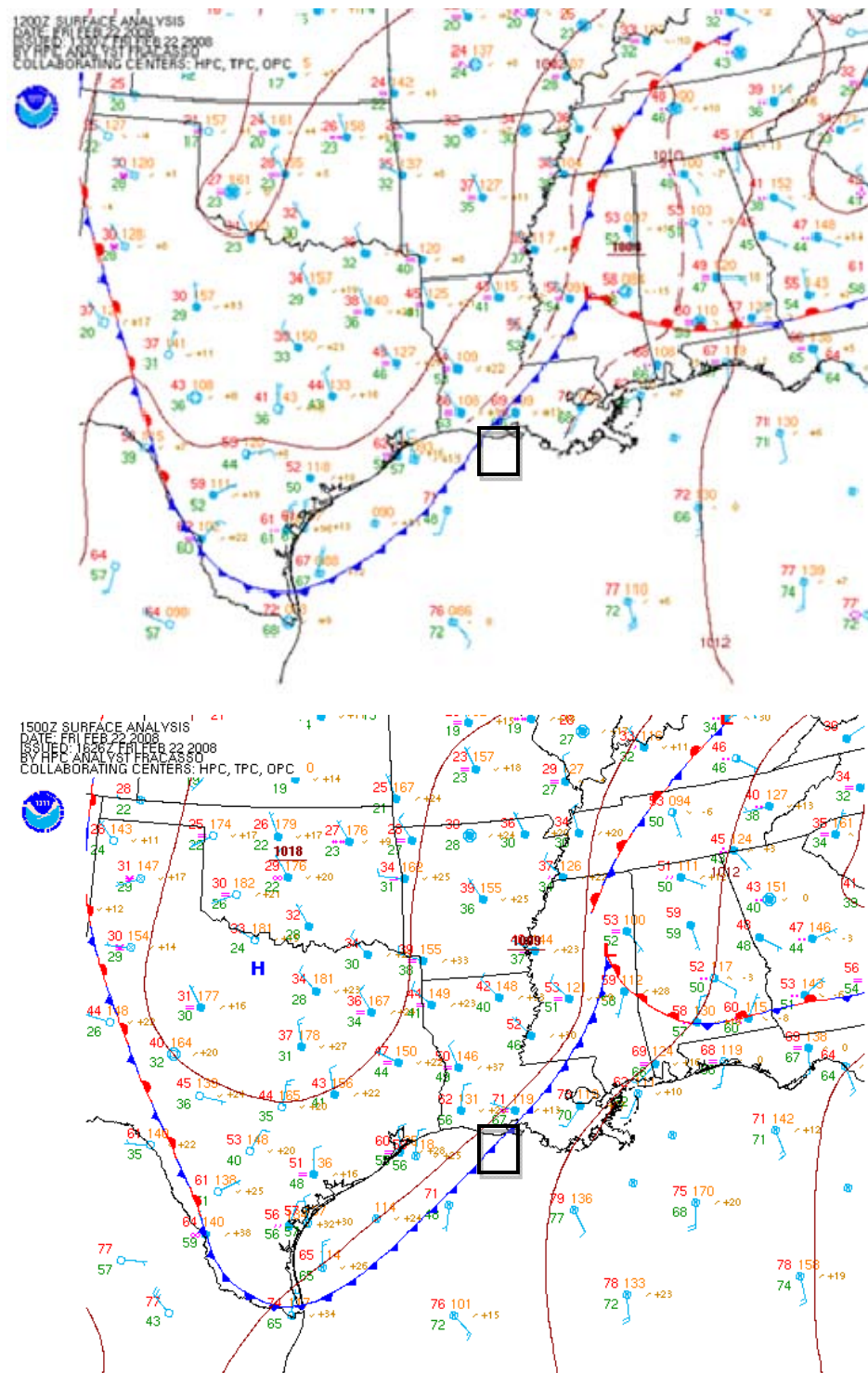
Figure 13.   Surface Analysis Weather Charts for February 22, 2008: 1200Z (Top panel)
and 1500Z (Bottom panel). (Same format as Figure 12) (From
nomads.ncdc.noaa.gov)
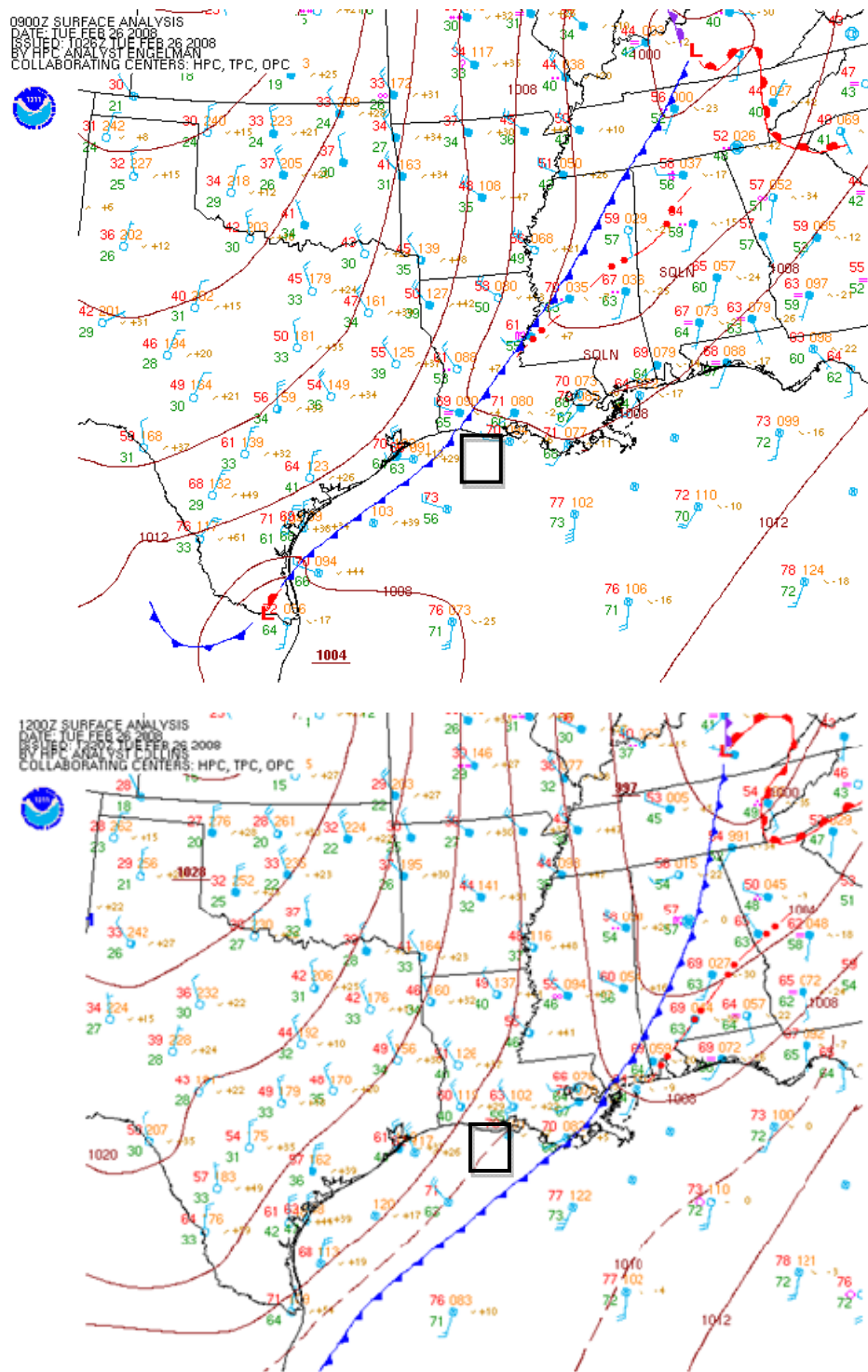
Figure 14.   Surface Analysis Weather Charts for February 26, 2008: 0900Z (Top panel)
and 1200Z (Bottom panel). (Same format as Figure 12) (From
nomads.ncdc.noaa.gov)
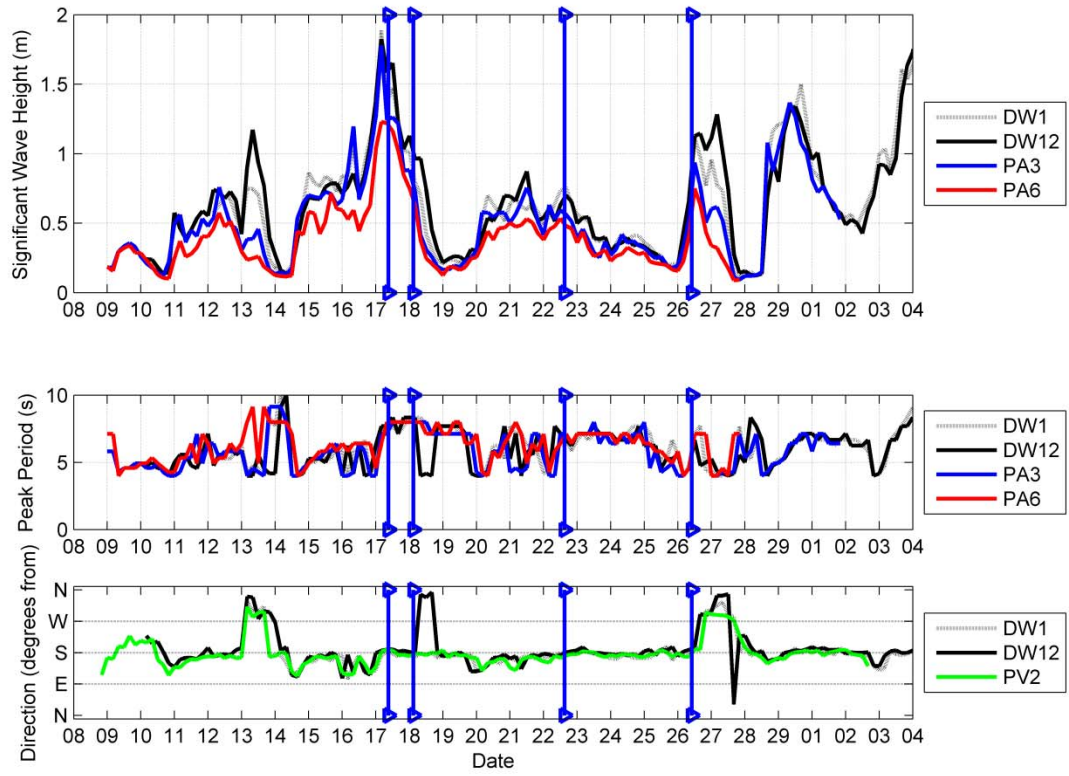
Figure 15.　　Wave observations for the western transect. Significant wave height H_s (Top panel). Peak period T_p (Middle panel). Peak wave direction D_p (Bottom panel). Cold fronts are marked by blue vertical lines.
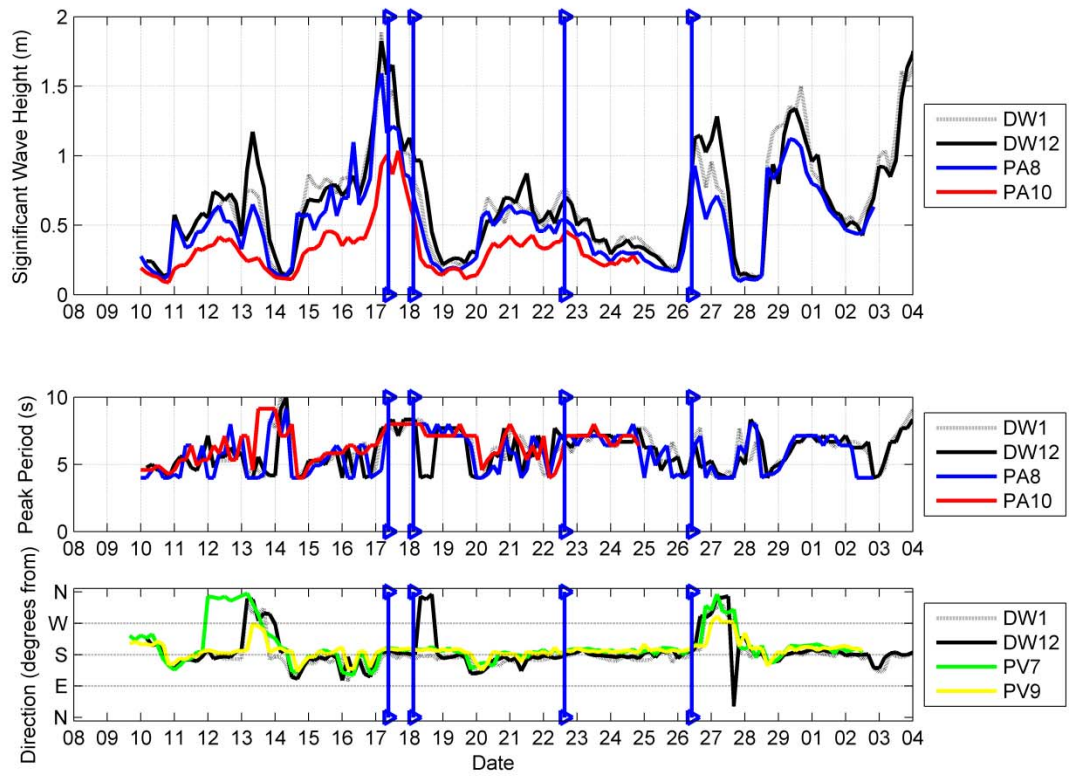
Figure 16.   Wave observations for the central transect. (Same format as Figure 15)
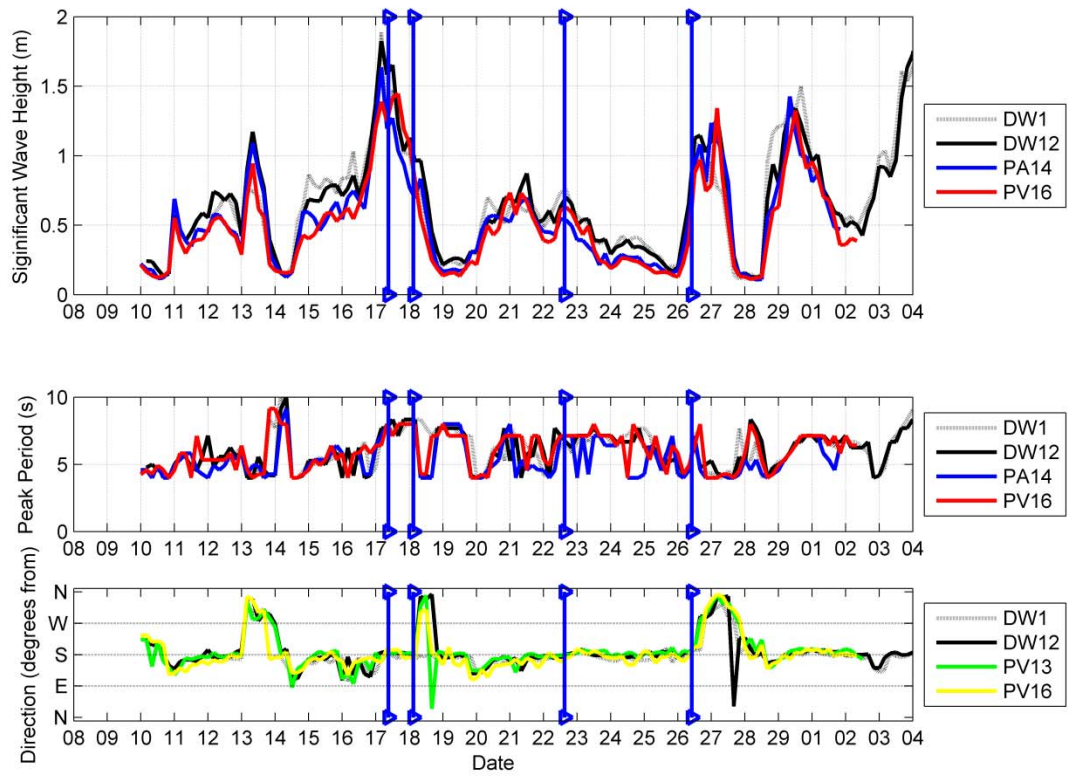
Figure 17.   Wave observations for the eastern transect. (Same format as Figure 15)
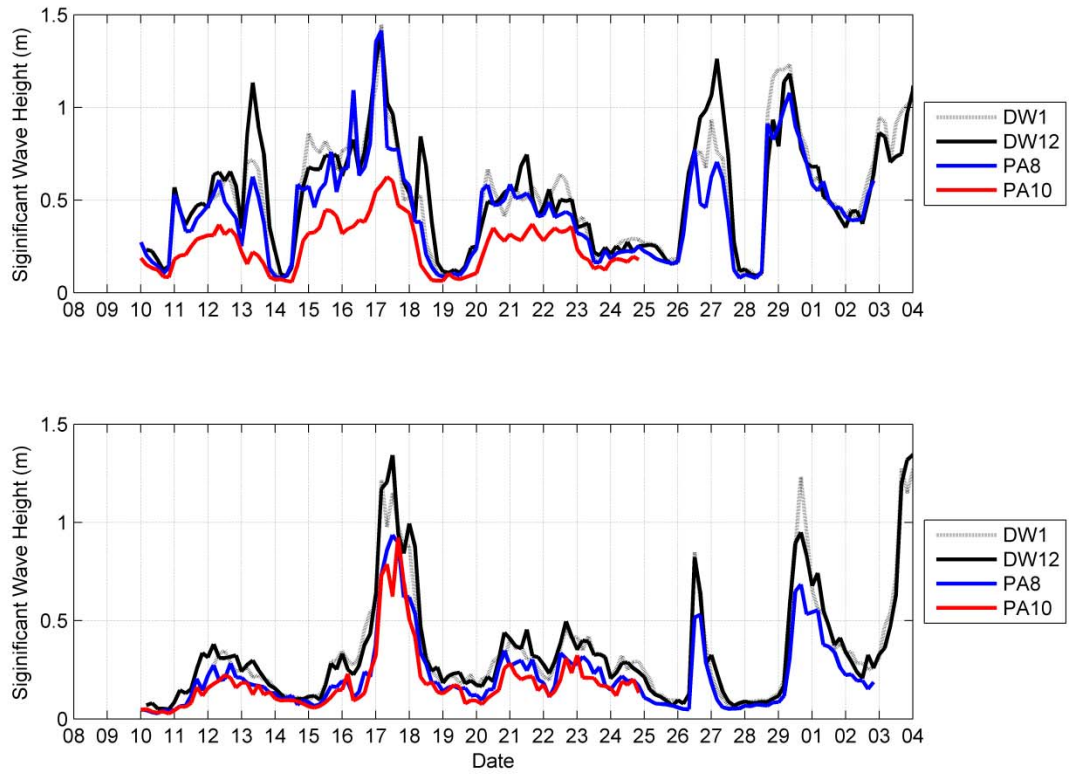
Figure 18.   Wave observations for the central transect. Sea component of significant wave height H_s (sea) (Top panel). Swell component of significant wave height H_s (swell) (Bottom panel).

V. SWAN MODEL IMPLEMENTATION

A. INTRODUCTION

Simulating WAves Nea rshore (SWAN) is a two-dim ensional, third-generation, spectral wave m odel de veloped by Delft Univ ersity of Technology (Booij et al., 1999). A third-generation m odel predicts wave spect ra evolution without any prior assumption of spectral shape. The standard SWAN model is an open source community model that is widely used by scientis ts and engineers to obtain estim ates of wave parameters in coastal areas, lakes and estuaries from a specifi ed wind field, bottom topography and input ambient currents (Holthuijsen et al., 2007). It is also commonly used around the world in military forecasting cen ters to ob tain predic ted wave heights before a m ilitary oper ation in the litto ral environm ent. This chapter will pr ovide a brie f descriptio n of the SWAN model and detail its implementation for MUDEX.

B. MODEL DESCRIPTION

The governing equation of the SWAN model used for MUDEX is the steady state energy balance equation in spherical coordinates described in Holthuijsen (2007):

$$\frac{\partial c_{g,\lambda} E(f,\theta;\lambda,\varphi)}{\partial \lambda} + \left(\cos\varphi\right)^{-1} \frac{\partial c_{g,\varphi} E(f,\theta;\lambda,\varphi)}{\partial \varphi}$$
$$+ \frac{\partial c_{\theta} E(f,\theta;\lambda,\varphi)}{\partial \theta} = S(f,\theta;\lambda,\varphi) \tag{13}$$

where $E(f,\theta)$ is th e energy density spectru m in term s of wave frequency f and wave direction θ. The first and second term on the left hand side of (13) represent the wave energy flux gradients associated with advection in latitude (φ) and longitude (λ) geographic space. The third term   represents d epth-induced refraction. The right hand side of (13) represents the total sour ce/sink te rm for the en ergy density. It accounts for the effects of generation, nonlinear wave-wav e interactions and dissipation. It is generally written as the sum of a num ber of separate source term s, each representing a different type of process:

$$S(f,\theta) = S_{in}(f,\theta) + S_{ds}(f,\theta) + S_{nl}(f,\theta) \tag{14}$$

where S_{in} represents wave generation by wind, S_{nl} is the wave energy transfer between spectral components due to nonlinear wave-wave interactions (including both quadruplet and triad interactions), and S_{ds} is the dissipation of wave energy due to whitecapping, wave-bottom interactions and depth induced breaking.

C.   BOTTOM DISSIPATION

The standard version o f SWAN does   not exp licitly acco unt for m ud-induced wave-damping but instead contai ns various formulations of bottom friction over a rigid sandy seabed that is considered the   dominant bottom dissipation m echanism for continental shelf seas with sandy bottom   s. The   default bottom   dissipation parameterization in SW AN is the widely us   ed em pirical JONSW AP bottom f riction model of Hasselmann et al. (1973) that takes th e form of a si mple linear source term (see Holthuijsen, 2007 for a review):

$$S_{bfr}(f,\theta) = -\frac{C_{bfr}}{g^2}\left[\frac{2\pi f}{\sinh(kh)}\right]^2 E(f,\theta) \tag{15}$$

where C_{bfr} is a (dim ensional) tuning param eter. Hasselm ann et al., (1973) suggested C_{bfr}=0.038 m^2/s^3 for swell conditions and Bouw s and Kom en (1983) suggested C_{bfr}= 0.067 m^2/s^3 for wind-sea conditions, the latter va   lue was im plemented as the def ault setting in SWAN.

There are two other bottom   friction m odels available in SWAN: the drag law model of Collins (1972) and the ed dy-viscosity model of Madsen et al. (1988). In this study we use the sim pler JONSWAP for mulation because the physics of m ud-induced wave damping are not captured by any of thes e models, and thus a simple linear damping term with a tunable coefficient provides a   sensible starting point to investiga te the observed damping rates over a muddy seafloor.

D. MODEL IMPLEMENTATION

SWAN Cyc le III version 40.51AB was im plemented in this study. The m odel was run in a two-dimensional stationary m ode on a spatia l g rid a nd f ormulated in spherical co ordinates. A sm all m odel domain of 34km (longitude) by 66km (latitu de) was selected with a unifor m rectan gular grid to cover th e western and central tran sects (Figure 19). Default settings were used for the source term param eterizations of wind forcing, quadruplet wave-wave interaction s, whitecapping dissipation an d depth ind uced breaking (H olthuijsen et al., 2007). However, different values of the tuning param eter C_{bfr} in the linear JONSWAP bottom friction source term were used to investig ate optimal model settings that match the wave dissipation observed at the field site.

As discussed in Chapter IV, the wind fi eld can be considered hom ogeneous for this relatively small model domain. The wind speed and direction were averaged for a 60 minute period centered on the m odel run start time. The averag ed v alue for the wind speed was then corrected to U_{10} (10m elevation) using a logarithm ic profile and Charnock's (1955) param eterization of sea surface rou ghness. A high reso lution bathymetry data set was interpolated ont o the model domain (Figure 19). Frequency directional spectra were estim ated fr om buoy DW12, using the MEM method by Lygre and Krogstad (1986) (see Chapter III), and a pplied as the offshore boundary condition on the southern side of the model domain.

The m odel was run with 60 frequency bands spaced logarithm ically over a frequency range of 0.04 Hz to 1.0 Hz. The dir ection resolution of the model was set at 5 degrees (72 bins). The cross shore spatia l resolution was set at 131m (250 m eshes) and the along shore spatial resolution was set at 137m (500 meshes).
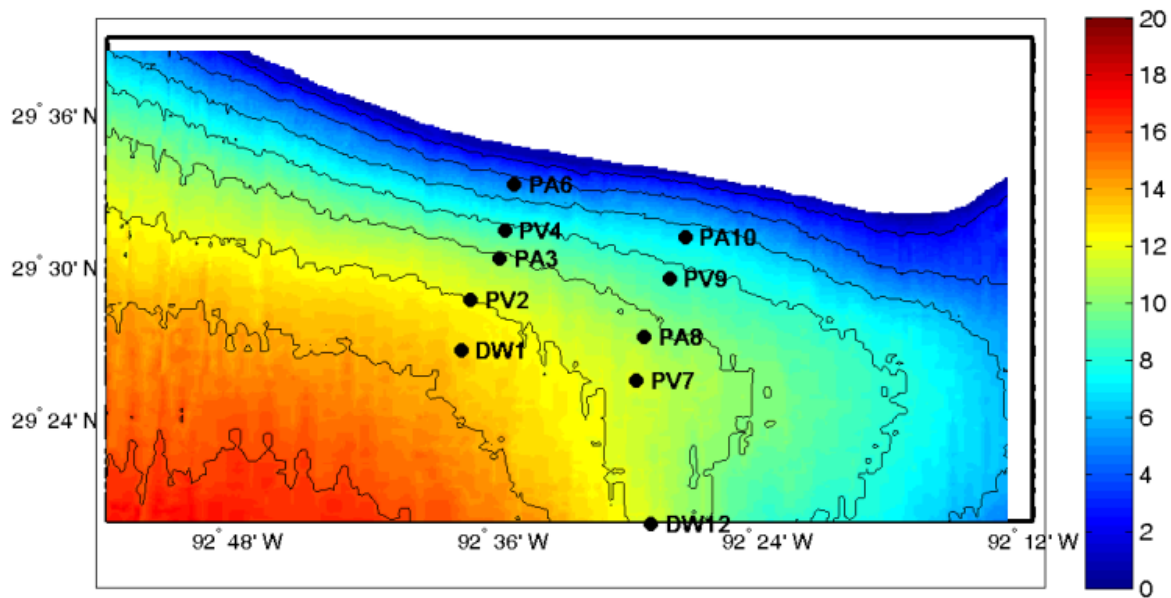
Figure 19.   SWAN model domain for MUDEX with instrument locations and depths in color (units m). Depth contours at 2m intervals.

VI. MODEL RESULTS

A.   INTRODUCTION

In th is ch apter, the ob servational r esults f rom MUDEX in Chapter IV will be compared to SWAN model predictions (descr ibed in Ch apter V). Specif ically, this chapter will evaluate the standard SWAN model's performance in a muddy environment. It will also exam ine an optim al value for the tuning coefficien t (C_{bfr}), in the bottom friction model of Hasselmann et al. (1973), to match wave damping at the field site.

Four case s tudies were carefully selected to rep resent dif ferent wind co nditions (Cases I and III - easterly, Case II - northwesterly and Case IV - no wind) (Figure 20). A steady southerly swell was also present in Cases I, III and IV. Case II was a fetch limited case with a building northwesterly wind sea. Wind conditions were relatively steady for each case with Case I chosen nine hours before the first front, Case II nine hours after the second front, Case III du ring a stationary ridge of high pressure and Case IV three h ours before the third front (Figure 20 T op panel). Input wind conditions for the m odel used average wind speed and direction observati ons over a one hour peri od, centered on the start of the wave observati on records. W ind speeds obser ved during the preceding and following one-hour periods did not deviate m ore than 2.8 m /s from the input conditions for all case studies.

The offshor e frequency-directional spect rum was estim ated from the waveride r buoy at site 12 (described in Chapter III) a nd implemented as the boundary condition on the sou thern side of the m odel dom ain f or a ll c ases. T his was co nsidered to be a reasonable assumption as the alongshore wave height variations obs erved on the eastern transect are much s maller than the cross-shore variations along the western and central transect (compare Figure 17 w ith Figures 15 and 16). This is further supported by wave energy spectra for the eastern transect (not shown) which are similar at all sites.

Wave conditions display som e te mporal va riation in wave height for each case study. This is particularly evident with Case s I and II during the pass age of the first two fronts as shown in Figure 20 (T op Panel). However, a closer analysis of the tran sects, shows that the observed wave heights do not vary m ore than 0.2 m for all case studies within a one hour period before or after m odel start tim e. Therefore, wave heights are considered reasonably steady to conduct model predictions at the selected times.

B.   CASE STUDIES

1.   Case I—Easterly Wind 0000Z February 17, 2008 (High Energy)

Case I represents a high energy southerl y swell with strong easterly winds nine hours before a frontal passage (Figure 20 Top Panel). An average wind direction of 102 degrees and wind speed of 12.4 m /s was computed from wind observations between 1630Z and 1730Z on February 17, 2009. Figure 21 shows the predicted significant wave height and peak direction acr oss the m odel domain. The dom inant south-easterly wave direction is fairly uniform across the dom ain, indicating refr action effects are weak, and differs by about 30 deg rees from the wind direction. The p redicted wave heigh ts decay with decreasing depth prim arily owing to th e bottom friction source term . Numerical errors in wave height and direction are appa rent on the eastern side of the m odel domain where the lateral boundary creates a shadow zone. These boundary effects occur in subsequent case studies but do not affect predicted wave pa rameters at th e ins trument sites as the domain is sufficiently large. This was further confirmed when the model was run on a much larger domain (not shown) with comparable results.

Observed energy spectra and m ean directions (θ_{mean}) as a function of frequency are com pared to m odel predictions for the western transect in Figure 22. The model prediction, using the default JONSWAP wind sea setting of $C_{bfr} = 0.067 \, m^2/s^3$, matches the observed spectral evolution fairly well. Figure 23 displays the sam e spectral information for the central transect. The mean direction (θ_{mean}) is well represented by the model, and the m odel captures the lo w frequency swell decay quite well. However, the considerable decay for high frequency wind waves a t the inshore sens ors, PV09 and

PA10, is not predicted by the m odel. The observed difference in high-frequency wave decay between the eas tern and central transect s may be related to th e greater extent of mud deposits found on the central transect that is in closer proximity to the outflow of the Atchafalaya river. The strong to gale force wind forcing obser ved offshore of the MUDEX area for three hours prior to the frontal passage (Figure 12 Top Panel) may have also played a ro le in s tirring up the water column and thus increas ing the fluidized mud content (see Sheremet and Stone, 2003; Jaramillo et al., 2009).

Predicted energy sp ectra are presen ted in Figure 24 for different values of the tuning parameter C_{bfr} in the JONSWAP bottom friction model. Increasing C_{bfr} enhances the dam ping of the low frequency swell peak but has no effect on the high-frequency wind-waves. This result illus trates a limitation of the standar d bottom damping term in SWAN that is based on the nea r-bed orbital wave motion (the $\sinh^2(kh)$ term in equation 13) and thus does not predict the decay of high frequency waves that are attenuated at the seafloor. T hese relatively short waveleng th waves m ay be dam ped by high sedim ent concentrations in the water co lumn, a process that is currently not rep resented in wave prediction models.

Figure 25 displays the com parison of obser ved wave heights to predicted wave heights for different bottom fr iction factors along both trans ects. The western tran sect shows little variation betw een the observations and model predictions with $C_{bfr} = 0.038\, m^2/s^3$ (swell setting) pro viding the b est agr eement with the observations . At the central transect the m odel cannot capture th e observed evolution with the zero friction ($C_{bfr} = 0\, m^2/s^3$) run matching only offshore observations (PV07 and PA08) and the $C_{bfr} = 0.09\, m^2/s^3$ run m atching only inshore observations (P V09 and PA10). The model does not reproduce the sharp reduction in wave height at the inshore sites, but inst ead predicts a more gradual decay that starts further offshore.

2. Case II—Northwesterly Wind 1200Z February 18, 2008 (Fetch Limited) single space vs. 1.5

Case II depicts fetch limited conditions with north westerly winds nine hours after a frontal passage (F igure 20 Top Panel). An average wind direction of 347 degrees and wind speed of 10.3 m /s was computed fr om wind observations between 1130Z and 1230Z on February 18, 2009. Model prediction s (Figure 26) show north-westerly wave propagation with wave heights increasi ng offshore as expected for fetch limited development. Sim ilar boundary effects, disc ussed in Case I, cause errors in wave direction along the western boundary.

Figure 27 displays observations and m odel predictions of energy spectra and mean directions vs. frequency for the wester n transect. Mo del predictions are b ased on the def ault bottom f riction setting ($C_{bfr} = 0.067 \ m^2/s^3$). Sim ilar to Case I, the model captures lo w f requency swell dec ay with n early con stant m ean direc tions f airly well. However, observations at the inshore sites show m uch l ower energy levels at high frequencies than is predicted. This appare nt suppression of high fr equency energy levels inshore is even m ore pronounced on the m uddier central transect (F igure 28). It appears that the muddy environm ent causes a dram atic slowing of the fetch lim ited wave development on the inner shelf that is very different from the predicted wave growth.

3. Case III—Easterly Wind 0400Z February 21, 2008 (Low Energy)

Case III rep resents a low energy southerly swell with easte rly winds (Figure 20 Top Panel) directed by a firm ridge of high pressure. An average wind direction of 64 degrees and wind speed of 8.8 m/s was computed from wind observations between 0330Z and 0430Z on February 21, 2009.

This case features a similar mix of southerly swell and easterly wind seas as Case I, but the en ergy levels are much lower. M odel-data comparisons for the central transect (Figure 29) show that the model, with default friction, captures the observed spectra and mean wave directions fairly well. The observed energy spectra sh ow slightly m ore damping of high frequencies at the inshor e sensor, PA10, than is predicted but the

48

difference is not as significant as in Case I. This result s upports the hypothesis by Sheremet and Stone (2003) that frontal passages may play a pivotal role in stirring up the sediment in the water column and damping high frequency waves.

The com parison of observed and predicted wave height varia tions (Figure 30) yields a sim ilar result as Case I. The m odel run with zero friction ($C_{bfr} = 0 \ m^2/s^3$) matches only offshore observations (PV07 and PA08) while the default friction ($C_{bfr} = 0.067 \ m^2/s^3$) run m atches the inshore observati on of PA10 but shows a m ore gradual cross-shore decay than is observed.

4. Case IV—No Wind 1200Z February 22, 2008 (Swell Only)

Case IV de picts a southerly swell with little to no winds (Figure 20 Top Panel) associated with a high pressure system over the area. An average wind direction of 295 degrees and wind speed of 1.5 m/s was computed from wind observations between 1130Z and 1230Z on February 22, 2009.

In these r elatively sim ple swell co nditions with nearly uni-directional onshore wave propagation, the m odel (using th e default bottom friction setting of $C_{bfr} = 0.067 \ m^2/s^3$) predicts a nearly uniform de cay of the spectrum and constant directions across the central tran sect that ag rees well with the ob servations (F igure 31). The observed and predicted wave heights along the central transect are com pared in Figure 32. As in previous cases, the model run with zero friction ($C_{bfr} = 0 \ m^2/s^3$) over-predicts the wave height. However, when the default bottom friction ($C_{bfr} = 0.067 \ m^2/s^3$) is used the predicted wave heights closely match the observations at all sites.

C. OVERALL MODEL PERFORMANCE

Overall, th e present re sults show that the d efault wind sea settin g ($C_{bfr} = 0.067 \ m^2/s^3$) for the JONSW AP bottom friction p arameterization used in the standard

SWAN model, gives reasonable estimates of significant wave heights that are satisfactory for most operational m ilitary purposes. Th e largest error in wave he ight prediction was 25 centimeters, at the shallowest site PA10 on the central transect, during Case I.

The comparison between observed and pred icted energy sp ectra showed that th e model (with def ault se tting $C_{bfr} = 0.067 \; m^2/s^3$) gener ally captur es the low f requency swell decay and matches the mean direction for each of the four case stu dies. However, the model failed to reproduce the appropriate level of high frequency wind wave damping for the central transect in Case I, both western and central transects in Case II and the central trans ect in Case III. Observations sho w wave da mping was stronges t on the central transect and in partic ular during Case I which invol ved the strongest winds. The model did not show the same variation between the transects.

The simple linear bottom friction model does not reflect a mud dissipation process and since its driven by near-bottom orbital wave motion it is effective only at damping low frequency swell peaks. W hen the syst em becom es bimodal with strong wind and swell conditions, the model fails to predict damping of high frequency waves.

Although only four case studies were examined, the dif ferent dam ping rates suggest that mud-induced dam ping of high frequency waves is enhanced when there is a strong frontal event. Frontal activity may stir up the water column fluidizing the mud and cause dissipation of high fr equency waves with short wave lengths that are de-coupled from seafloor processes. This m ay provide an additional dissipation m echanism that is different f rom the tradition al dir ect wave-b ottom interaction pro cesses. A bette r understanding of the physics of the mud suspension process and the associated increase in viscos ity is needed to param eterize th is ef fect in a co astal wave pr ediction m odel. Until this process is properly accounted fo r, the defau lt wind sea setting of the JONSWAP bottom friction model is recommended for operational purposes.

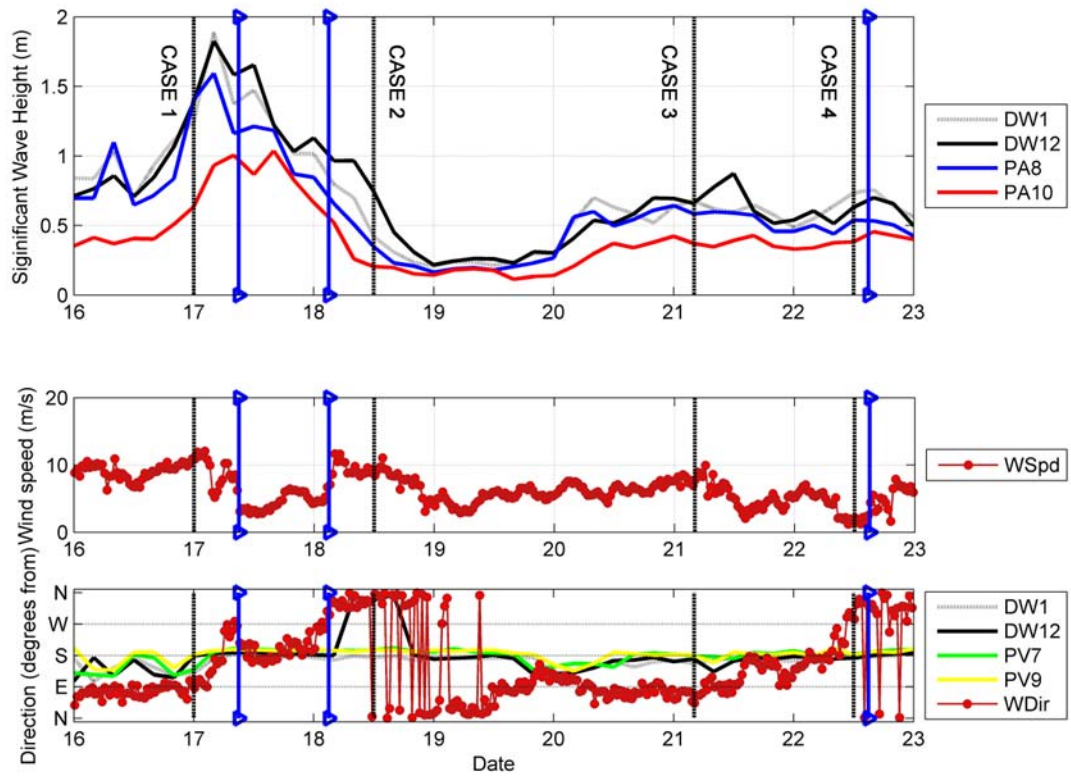Figure 20.   Wave and wind observations for the central transect displaying four case studies selected for analysis. Significant wave height H_s (Top panel). Wind speed (Middle panel). Peak wave direction D_p and wind direction (Bottom panel). Cold fronts are marked by blue vertical lines. Case studies are marked by black vertical lines. (Wind data courtesy of Dr. John Trowbridge and Dr. Janet Fredericks at WHOI)
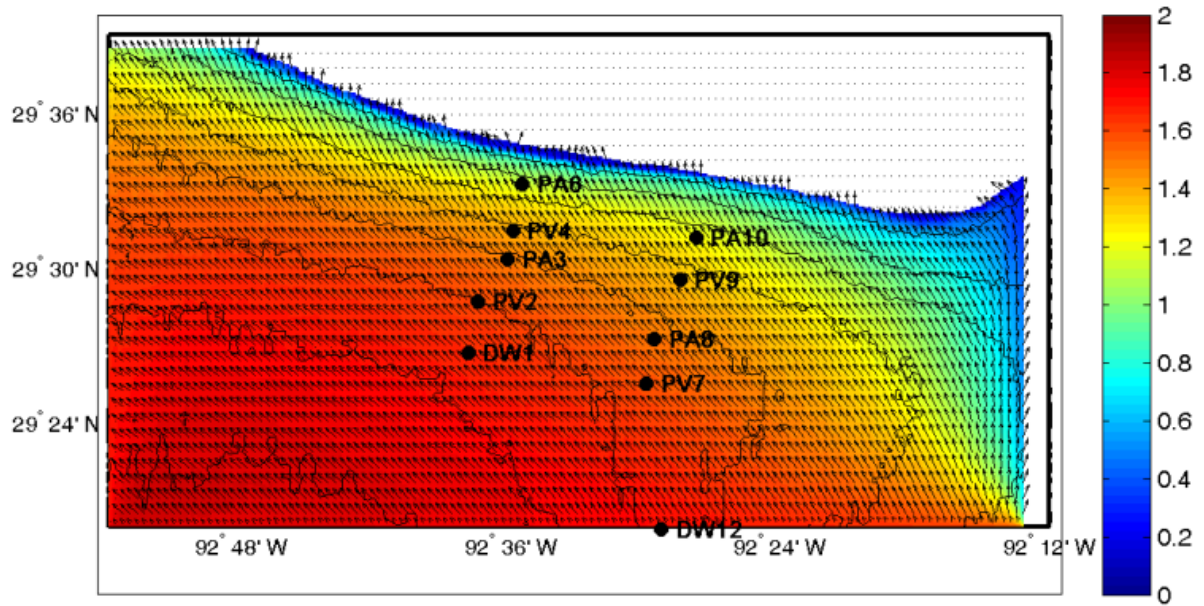
Figure 21.   SWAN Model output for Case Study I with instrument locations and significant wave height in color (units m). Depth contours at 2m intervals.
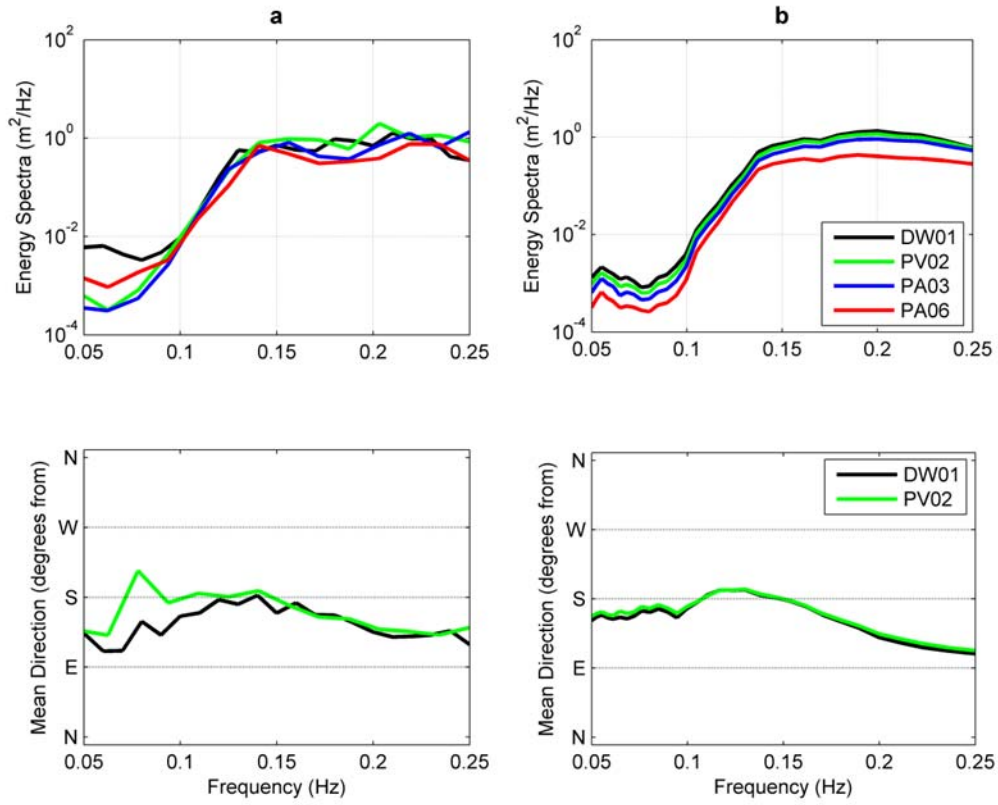
Figure 22.　　Case I model-data comparisons for the western transect using the default JONSWAP bottom friction source term (wind-sea setting, $C_{bfr} = 0.067\,m^2/s^3$). **a.** Observed wave energy spectra (Top panel) and mean direction vs. frequency (Bottom panel). **b.** Corresponding model predictions.

Figure 23.   Case I model-data comparisons for the central transect ($C_{bfr} = 0.067\,m^2/s^3$).
a. Observed. **b.** SWAN model prediction.   (Same format as Figure 23)
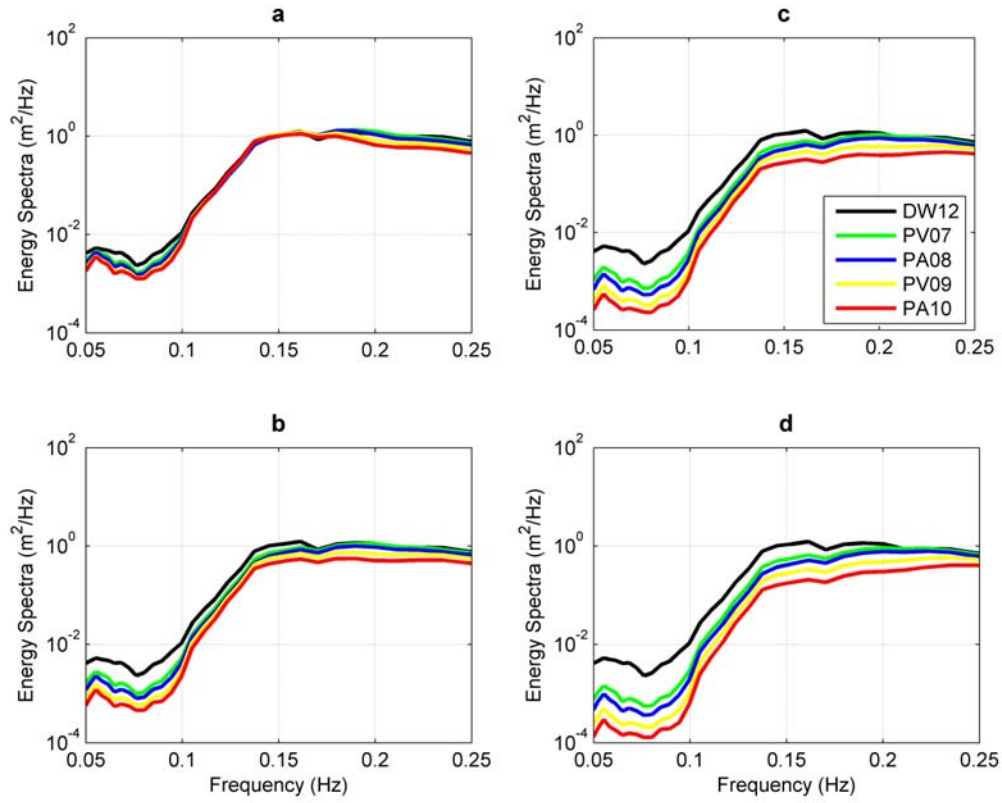
Figure 24. SWAN model predictions of wave energy spectra on the central transect for Case I using different values for the tuning parameter C_{bfr} in the JONSWAP bottom friction source term. **a.** $C_{bfr} = 0\,m^2/s^3$. **b.** $C_{bfr} = 0.038\,m^2/s^3$. **c.** $C_{bfr} = 0.067\,m^2/s^3$. **d.** $C_{bfr} = 0.09.\,m^2/s^3$
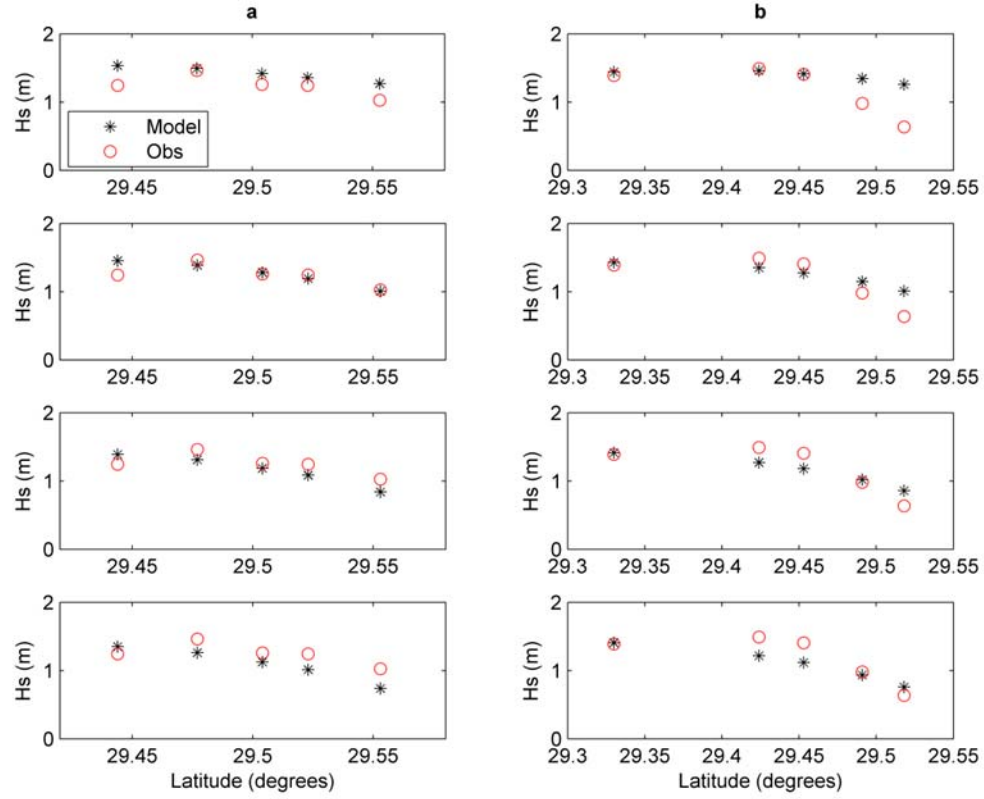
Figure 25. Comparison of observed significant wave heights and SWAN model predictions in Case I using different values of the bottom friction tuning parameter C_{bfr} : from top to bottom: $C_{bfr} = 0\,m^2/s^3$, $0.038\,m^2/s^3$, $0.067\,m^2/s^3$ and $0.09\,m^2/s^3$. **a.** Western transect (Sites from left to right are DW1, PV2, PA3, PV4 and PA6). **b.** Central transect (Sites from left to right are DW12, PV7, PA8, PV9 and PA10).
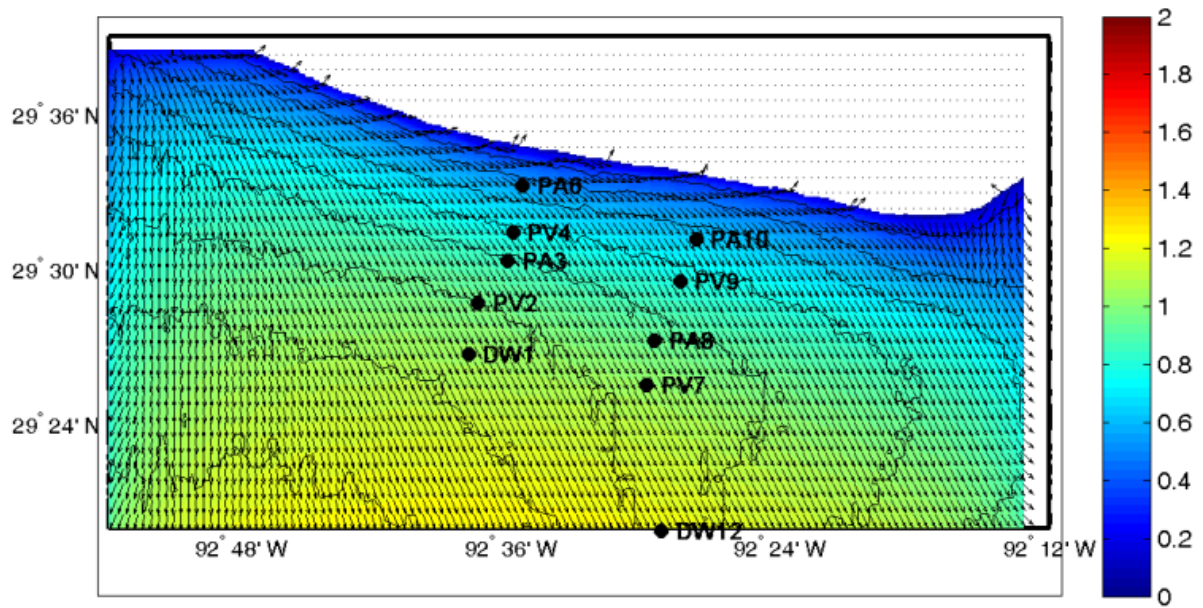
Figure 26.   SWAN Model output for Case Study II with instrument locations and significant wave height in color (units m). Depth contours at 2m intervals.
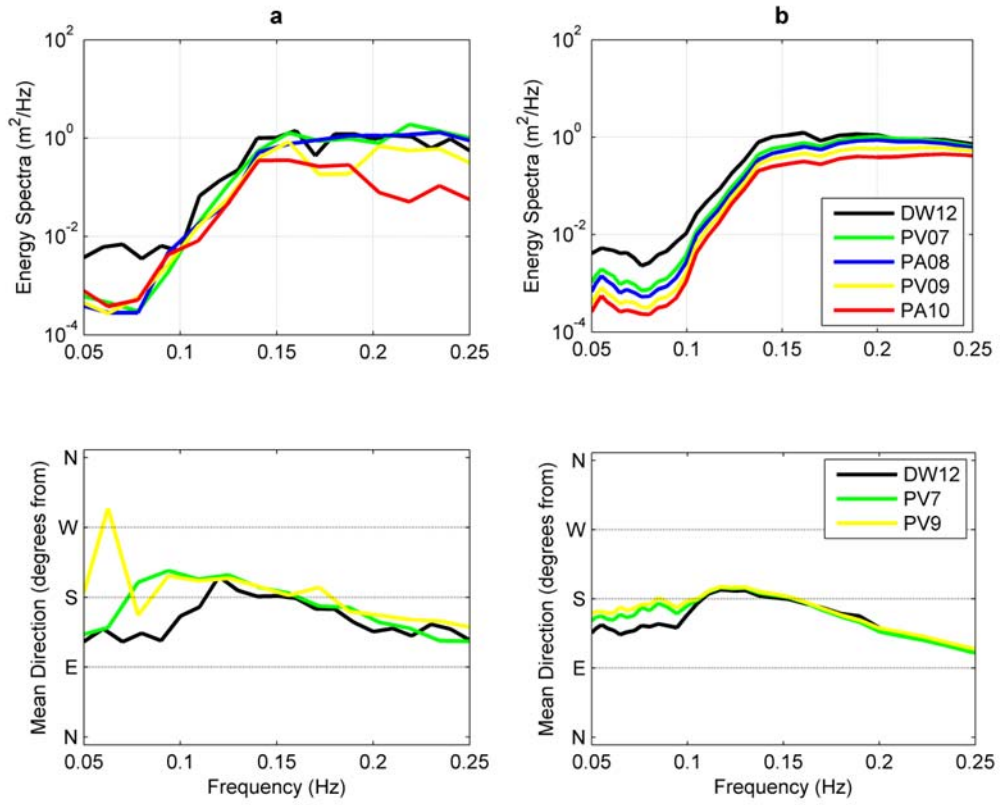
Figure 27.　　Case II model-data comparisons for the western transect ($C_{bfr} = 0.067\,m^2/s^3$).
a. Observed.　**b.** SWAN model.　(Same format as Figure 23)

Figure 28.　　Case II model-data comparisons for the central transect ($C_{bfr} = 0.067\,m^2/s^3$).
**a.** Observed. **b.** SWAN model. (Same format as Figure 23)

Figure 29. Case III model-data comparisons for the central transect ($C_{bfr} = 0.067\,m^2/s^3$). **a.** Observed. **b.** SWAN model. (Same format as Figure 23)

Figure 30.   Case III comparison of observed significant wave height and SWAN model predictions on the central transect using different tuning parameter (C_{bfr}) values in the JONSWAP bottom friction source term (Sites from left to right are DW12, PV7, PA8, PV9, PA10). $C_{bfr} = 0\, m^2/s^3$ (Top panel). $C_{bfr} = 0.067\, m^2/s^3$ (default wind sea setting) (Bottom panel).
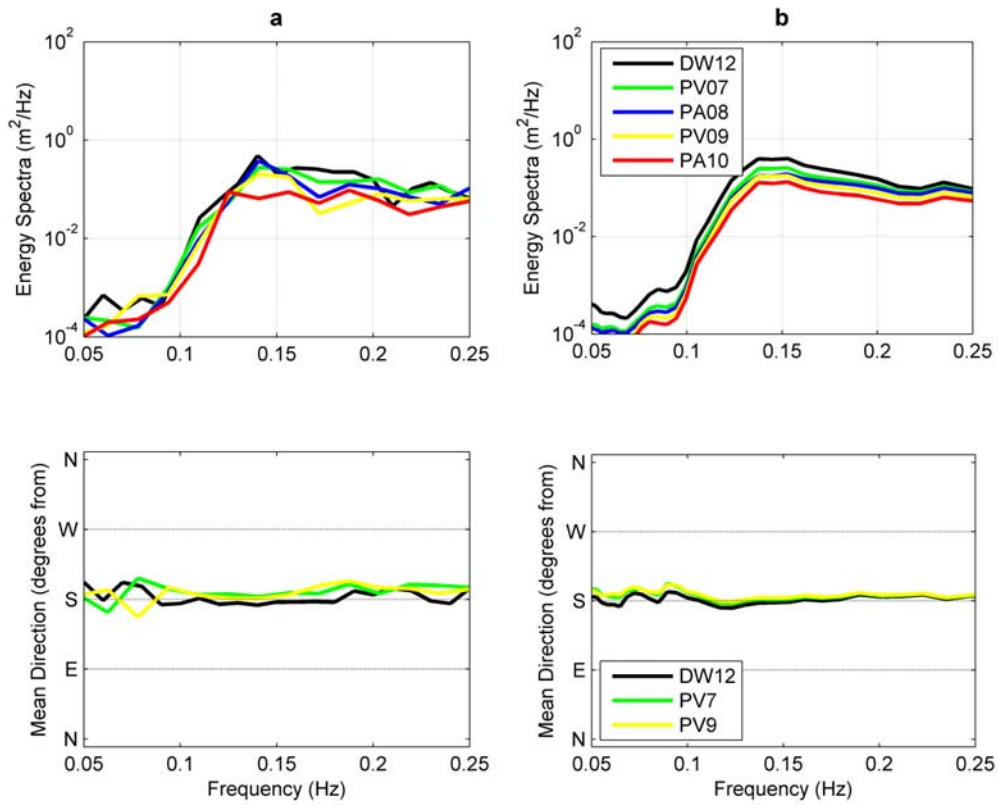
Figure 31.   Case IV model-data comparisons for the central transect ($C_{bfr} = 0.067\, m^2 \big/ s^3$).
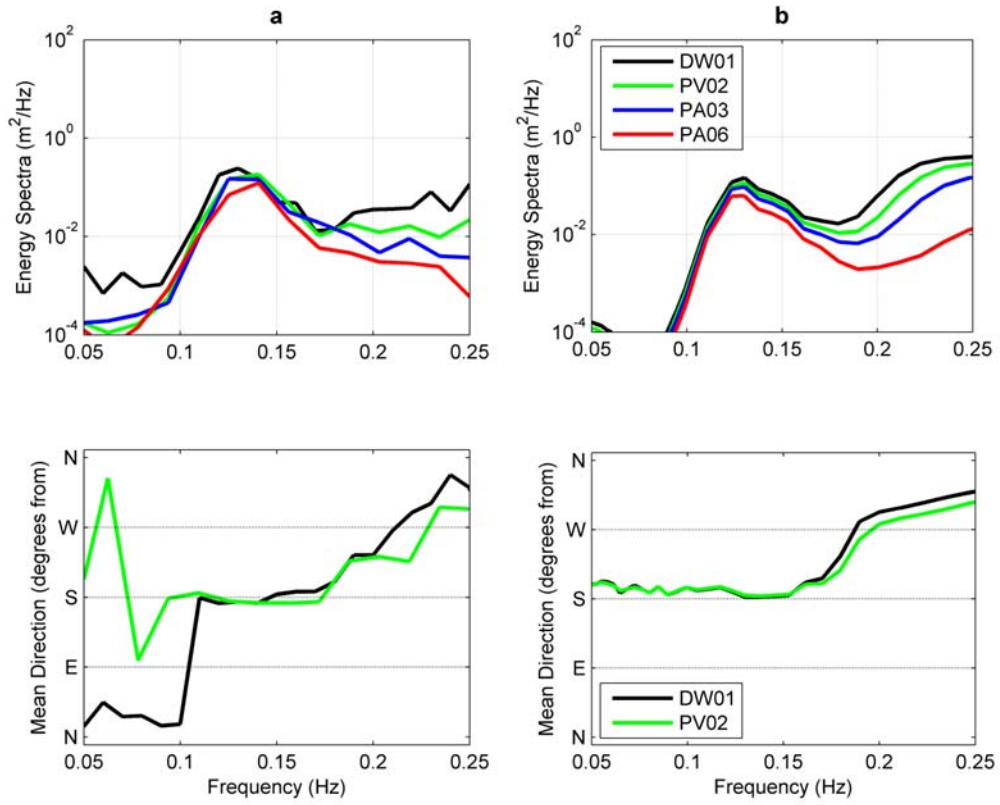**a.** Observed. **b.** SWAN model. (Same format as Figure 23)

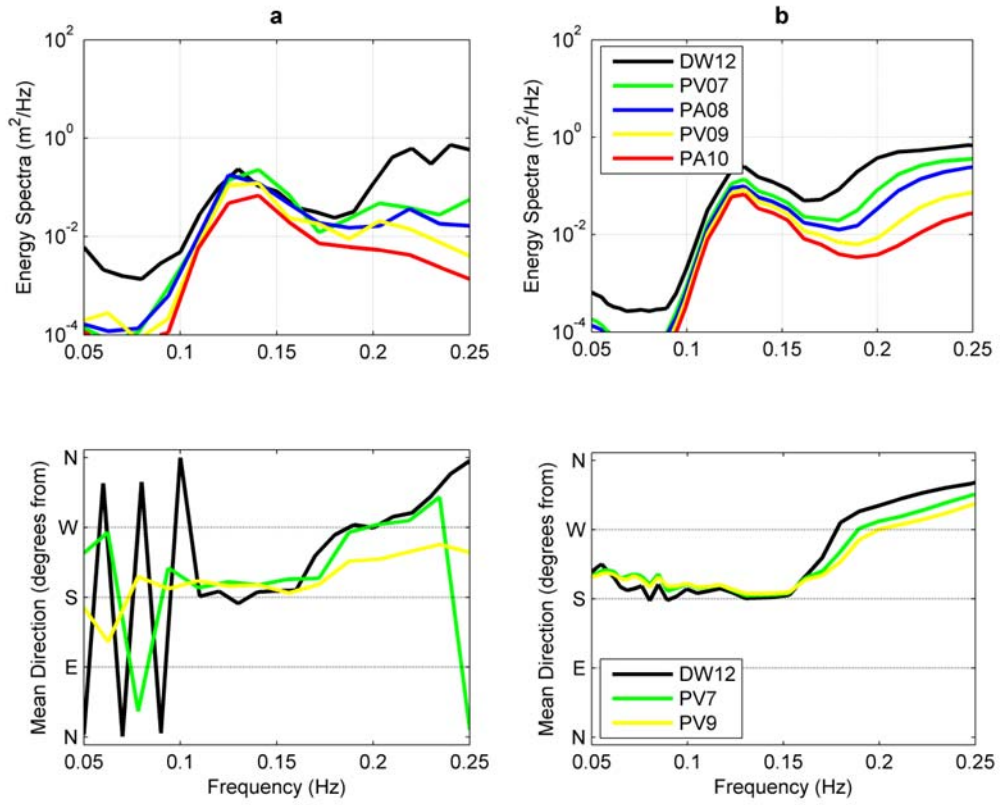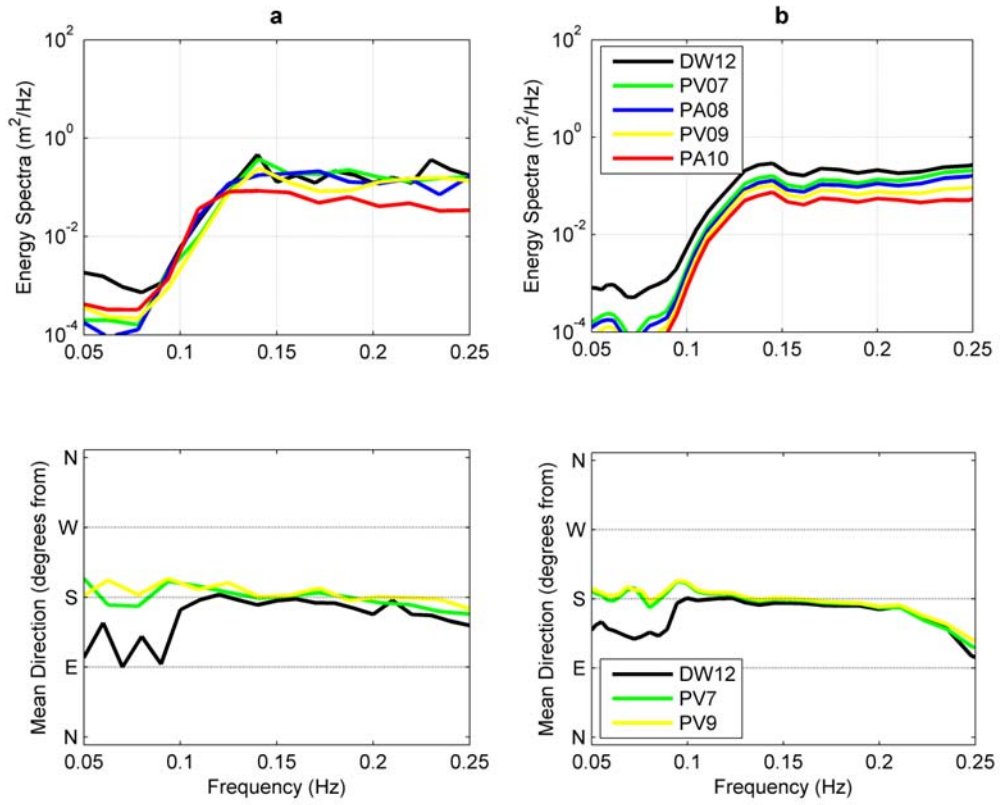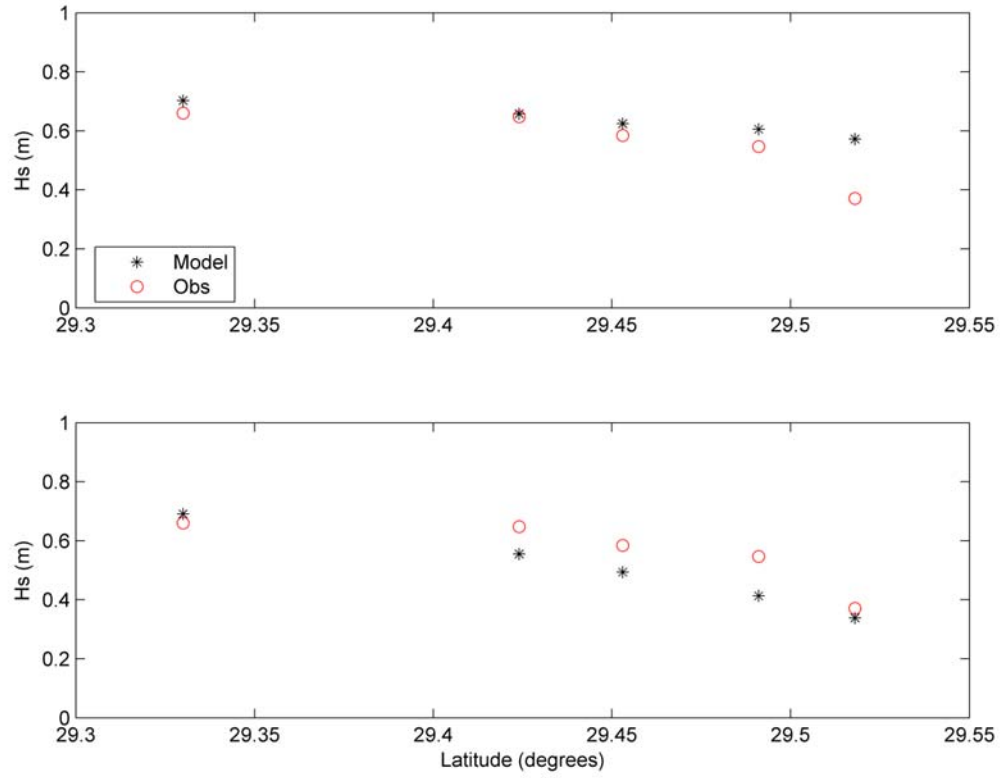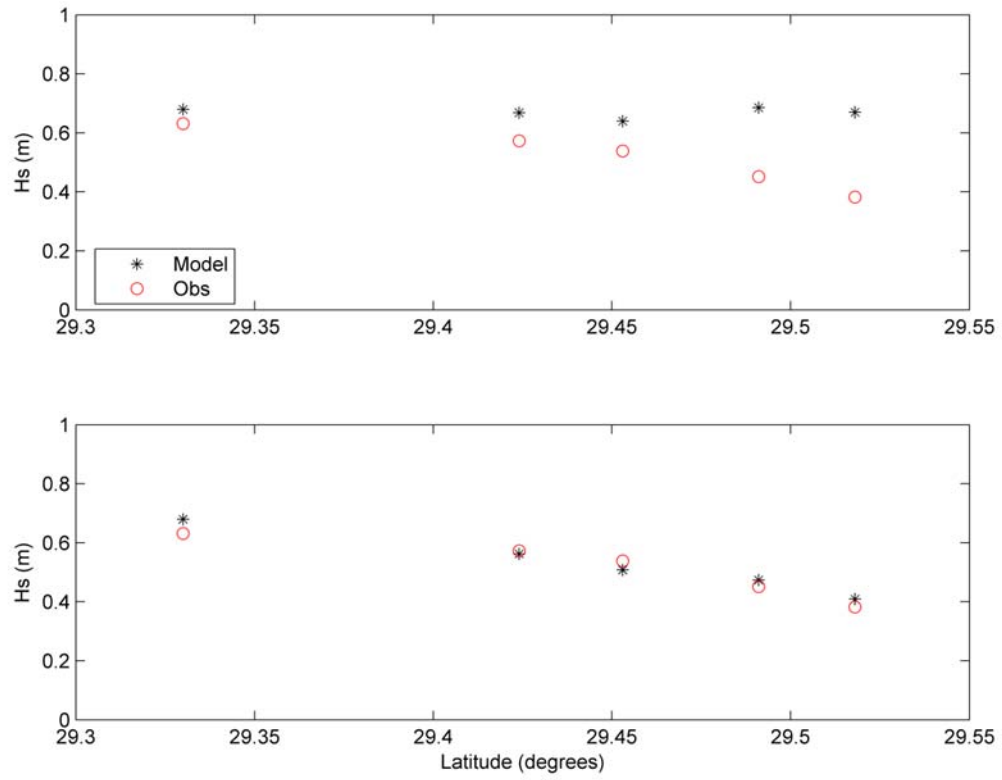Figure 32.   Case IV comparison of observed significant wave height and SWAN model predictions on the central transect. Top panel: no friction, Bottom panel: default $C_{bfr} = 0.067\,m^2/s^3$. (Same format as Figure 30)

THIS PAGE INTENTIONALLY LEFT BLANK

VII. SUMMARY AND CONCLUSIONS

The transformation of ocean surface waves acro ss the muddy continental shelf of Western Louisian a was exam ined with two m onths of extensive wa ve data co llected during the ONR-funde d Louisiana MUD EXpe riment (MUDEX) held in the late winter/early spring of 2008. The experim ent was designed to provide a com prehensive field data set for analysis of mud-indu ced wave damping and validation for an operational wave prediction m odel such as SWAN (Simulating WAves Nearshore). This thesis pres ents th e in itial analysis of the MUDEX observations and a com parison of observed and predicted wave param eters and spectra with SWAN predictions. Specifically, the overall performance of the SWAN model in its standard configuration is evaluated and a recom mendation for the optim al value of the tuning coef ficient in the bottom f riction param eterization (b ased on th e m odel of Hasselm ann et al., 1973) is given.

The MUDEX Experim ent included the deploym ent of 16 wave m easuring instruments between February-March, 2008, in depths ranging from 13 to 4m . The instruments included two directional waverider buoys, six bottom tripods equipped with a pressure-velocity sensor and a current profil er, and eight bottom tripods equipped with a pressure sensor. The two-dim ensional 40 by 25 km array consiste d of two cross-shore transects, named 'Western' and 'Central' and an alongshore transect named 'Eastern'.

Analysis of box core samples collected on the two cross-shor e transects showed there was a greater ex tent of soft mud (5-10 cm) and very soft fluid m ud (1-2 cm) on the central tran sect when co mpared to the wester n transect (soft m ud <5 cm and very soft fluid mud <1 cm). This was probably a direct result of the central transect being closer in proximity to the m uddy outflow of the At chafalaya Riv er. W ind observations and surface weather chart analysis sho wed that fr onts regu larly cross the area eve ry four to five days and cause increased wave heights due to increased wind fo rcing. Analysis of general wave observations along the cross-s hore transects showed a gradual decay along the western transect and a m uch sharper de cay at the shallowest instrum ents along the central transect. This sharper decay along the central transect m ay be attributed

to the thicker layer of mud m easured on that transect. The alongshore eastern transect observations showed much sm aller variations in wave heights than the cross-shore transects.

Four wind sea events were examined in detail along th e cross-shore transects and compared to SWAN model pred ictions (default bottom f riction s etting of $C_{bfr} =$ $0.067\, m^2/s^3$). The com parison between observed and predicted energy spectra for each event showed that the model generally captu res the low frequency swell decay fairly well. The model also approxim ately reproduced the observed m ean wave direction as a function of frequency. However, the obser ved considerable decay of high frequency wind-waves at the inshore sensors w as not ca ptured by the model. This high frequency decay was especially strong (as m uch as an order of m agnitude) on the central tran sect, when the wave field was bim odal with a str ong alongshore easterly wind in the presence of a high energy southerly swell. When th e alongshore wind-sea and swell subsided, the high energy frequency decay was less pronounced. Similar to the easterly winds case, the model also under-predicts energy levels at hi gh frequencies during periods of offshore north-westerly winds. In this fetch lim ited regim e the observa tions show strong suppression (up to two orders of m agnitude) of high frequency energy levels inshore on both the western and central tr ansect, although this is slig htly m ore prom inent on the muddier central transect. It is apparent that the muddy environm ent causes a dram atic slowing of the fetch limited sea development in shallow water.

Analysis of different values of the t uning parameter (C_{bfr}) in the bottom friction parameterization showe d that incre asing the va lue of C_{bfr} enhances the damping of the lower frequency swell com ponent of the wa ve spectrum, but has no ef fect on the high-frequency waves. In relatively simple sw ell conditions with no wind-sea, the model spectra closely m atched the observed spectra for the default value of 0.067 m^2/s^3 . However, tuning the value of C_{bfr} to the observed wave height decay in bimodal sea states yielded excessive damping of the swell co mponent and not enough da mping of the high-

feequency wind-sea. Clearly, the bottom friction model based on the drag exerted by the near-bed wave orbital motion cannot describe the observed dissipation of high-frequency wind-seas that are attenuated at the sea floor.

Overall, the comparison of observed and predicted significant wave heights for each event showed that the standard SWAN model, with the default bottom friction setting, gives reasonable results for most Navy littoral operations that require only wave height predictions. However, when there are alongshore winds, the model does not quite match the observed sharp reduction in wave height near the shore at the inshore sites, but instead predicts a more gradual decay that starts further offshore.

Although only four case studies were analyzed, results suggest that wave damping in shallow water is enhanced when there is a strong frontal event (strong easterly winds and high energy southerly swell). In shallow water the strong wind forcing before and during a frontal passage may fluidize the mud over the entire water column and the increased viscosity may cause high frequency wave dissipation, as suggested by Sheremet and Stone (2003) and Jaramillo et al., (2009). This may provide an additional dissipation mechanism that is different from the traditional bottom-induced mud dissipation process. While improvements of wave models requires new physics-based mud-induced dissipation mechanisms, at present the default settings for SWAN appear to provide a reasonable approximation of wave heights inshore of a muddy environment, and is recommended for use in military operations.

THIS PAGE INTENTIONALLY LEFT BLANK

LIST OF REFERENCES

Booij, N., Ris, R.C., & Holthuijsen, L.H. (1999). A third-generation wave model for coastal regions. 1. Model description and validation. *J. Geophys. Res., 104(C4),* 7469-7666.

Bouws, E., & Komen, G.J. (1983). On the balance between growth and dissipation in an extreme, depth limited wind-sea in the southern North Sea, *J. Phys. Oceanogr., 13,* 1653-1658.

Cuchiara, D.C., Fernandes, E.H., Strauch, J.C., Winterwerp, J.C., & Calliari, L.J. (2009). Determination of the wave climate for the southern Brazilian shelf. *Cont. Shelf Res., 29,* 545-555.

Charnock, H. (1955). Wind stress over a water surface. *Quart. J. Roy. Meteorol. Soc., 81,* 639–640.

Dalrymple, R., & Liu, P. (1978). Waves over soft muds: A two-layer fluid model. *J. Phys. Oceanogr., 8,* 1121-1131.

De Wit, P.J. (1995). *Liquefaction of cohesive sediment by waves.* Ph.D. dissertation. Delft University of Technology, the Netherlands.

Dingemans, M.W. (1998). *A review of of the physical formulations in SWAN* (p. 69). Delft Hydraulics Report H3306, Delft, the Netherlands.

Elgar, S., & Raubenheimer, B. (2008). Wave dissipation by muddy seafloors. *Geophys. Res. Letters, 35,* LO7611, pp. 1-5.

Flemming, B.W., Delafontaine, M.T., & Liebezeit, G. (2000). *Muddy coast dynamics and resource management* (p. 99). Elsevier, University of Michigan.

Gade, H. (1958). Effects of a non-rigid, impermeable bottom on plane surface waves in shallow water. *J. Mar. Res, 16*, 61-82.

Garcia-Garcia, A., et al. (2008). A geophysical baseline for the Fluid-Mud MURI site, west of Atchafalaya Bay, *Geo. Mar. Letters*, (submitted).

Hasselmann, K., et al. (1973). Measurements of wind-wave growth and swell decay during the Joint North Sea Wave Project (JONSWAP). *Dtsch. Hydrogr. Z. Sup., A8(12),* 95.

Herbers, T.H.C., Elgar, S., Guza, R.T. (1999) Directional spreading of waves in the nearshore. *J. Geophys. Res., 104(C4),* 7683-7693.

Holthuijsen, L.H. (2007). *Waves in Oceanic and Coastal Waters* (1 st ed) (pp.288-289). Cambridge University Press, New York.

Holthuijsen, L.H., et al. (2007). *SWAN Cycle III version 40.51AB User Manual*, from http://www.fluidmechanics.tudelft.nl/swan/default.htm

Hsiao, S., & Shemdin, O. (1980). Interaction of ocean waves with a soft bottom. *J. Phys. Oceanogr., 10,* 605-610.

Jaramillo S., Sherem et, A., Allison, M.A., Reed, A.H., & Holland K.T. (2009). Wave-mud interactions over the muddy Atchafalaya subaqueous clinoform, Louisiana, United States: Wave-supported sediment transport. *J. Geophys. Res., 114,* C04002, doi:10.1029/2008JC004821.

Komen, G.J., Cavaleri, L., Donelan, M., Hasselmann, K., Hasselmann, S., & Janssen, P.A.E.M. (1994). *Dynamics and Modelling of Ocean Waves* (p. 532). Cambridge University Press, New York.

Longuet-Higgins, M.S., Cartwright, D.E., & Smith, N.D. (1963). Observations of directional spectrum of sea waves using the motions of a floating buoy. In Ocean Wave Spectra, *Proceedings of a Conference,* Easton, Maryland, National Academy of Sciences, Prentice Hall, 111-136.

Lygre, A., & Krogstad, H.E. (1986). Maximum entropy estimation of directional distribution in ocean wave spectra. *J. Phys. Oceanogr, 16,* 2052-2060.

MacPherson, H. (1980). The attenuation of water waves over a non-rigid bed. *J. Fluid Mech., 97,* 721-742.

Mei, C., & Liu, P. (1987). A Bingham-plastic model for a muddy sea bed under long waves. *J. Geophys. Res., 92,* 14,581-14,594.

Mossa, J., & Roberts, H.H. (1990). Synergism of riverine and winter storm-related sediment transport processes in Louisiana's coastal wetlands. *Gulf Coast Assoc. of Geological Soc. Trans., 40,* 635-642.

Ng, C., (2000). Water waves over a muddy bed: A two layer Stokes' boundary layer model. *Coastal Eng., 40,* 221-242.

O'Reilly, W.C., Herbers, T.H.C., Seymour, R.J., & Guza, R.T. (1996). A Comparison of Directional Buoy and Fixed Platform Measurements of Pacific Swell. *J. of Atmospheric and Oceanic Technology, 13(1),* 231-238.

Piedra-Cueva, I. (1993). On the response of a muddy bottom to surface water waves. *J. of Hydraulic Research, 31(5),* 681-696.

Rogers, E.W., & Holland, T.K. (2009). A study of dissipation of wind-waves by mud at Cassino Beach, Brazil: Prediction and inversion. *Cont. Shelf Res., 29,* 676-690.

Sheremet, A., & Stone, G.W. (2003). Observations of n earshore wave dissipation over muddy sea beds. *J. Geophys. Res., 108(C11),* 3357, doi:10.1029/2003JC001885.

Tolman, H.L., & Chalikov, D. (1996). Sour ce term s in a third-generation wind-wave model. *Journal of Physical Oceanography, 26,* 2497-2518.

Tubman, M.W ., & Suhayda, J.N. (1976). W ave action and bottom movem ents in fine sediments. *Proc. 15th Coastal Eng. Conf.,* ASCE, Honolulu, 1168-1183.

U.S. Department of the Navy. (1992). *From the sea: Preparing the Naval Service for the 21st Century.*

U.S. Department of the Navy., & U.S. Coast Guard. (2007). *A Cooperative Strategy for 21st Century Seapower.*

Winterwerp, J.C., de Graff, R.F., Groeneweg, J., & Luijendijk, A.P. (2007). Modelling of wave damping at Guyana mud coast. *Coastal Eng., 54,* 249-261.

THIS PAGE INTENTIONALLY LEFT BLANK

INITIAL DISTRIBUTION LIST

1. Defense Technical Information Center
   Ft. Belvoir, Virginia

2. Dudley Knox Library
   Naval Postgraduate School
   Monterey, California

3. Professor T. H. C. Herbers, Department of Oceanography (Code OC/He)
   Naval Postgraduate School
   Monterey, California

4. Assistant Professor Tim T. Janssen, Department of Geosciences
   San Francisco State University
   San Francisco, California

5. Mr. Paul Jessen, Department of Oceanography
   Naval Postgraduate School
   Monterey, California

6. CMDR Robert H. Woodham
   Directorate of Oceanography and Meteorology
   Sydney, NSW, Australia

7. LCDR Lincoln Trainor
   Directorate of Oceanography and Meteorology
   Sydney, NSW, Australia